In focus

Insights into the interstitium of ventricular myocardium: interstitial Cajal-like cells (ICLC)

L.M. Popescu [a,b] *, **Mihaela Gherghiceanu [a]**, **M.E. Hinescu [a,b]**, **D. Cretoiu [a,b]**, **Laura Ceafalan [b]**, **T. Regalia [b]**, **A.C. Popescu [b]**, **Carmen Ardeleanu [a]**, **E. Mandache [a]**

[a] *'Victor Babeⁿ' National Institute of Pathology, Bucharest, Romania*
[b] *Department of Cellular and Molecular Medicine,*
'Carol Davila' University of Medicine and Pharmacy, Bucharest, Romania

Abstract

We have previously described interstitial Cajal-like cells (ICLC) in human atrial myocardium. Several complementary approaches were used to verify the existence of ICLC in the interstitium of rat or human ventricular myocardium: primary cell cultures, vital stainings (*e.g.*: methylene blue), traditional stainings (including silver impregnation), phase contrast and non-conventional light microscopy (Epon-embedded semithin sections), transmission electron microscopy (TEM) (serial ultrathin sections), stereology, immunohistochemistry (IHC) and immunofluorescence (IF) with molecular probes. Cardiomyocytes occupy about 75% of rat ventricular myocardium volume. ICLC represent ~32% of the number of interstitial cells and the ratio cardiomyocytes/ICLC is about 70/1. In the interstitium, ICLC establish close contacts with nerve fibers, myocytes, blood capillaries and with immunoreactive cells (stromal synapses). ICLC show characteristic cytoplasmic processes, frequently two or three, which are very long (tens up to hundreds of μm), very thin (0.1–0.5μm thick), with uneven caliber, having dilations, resulting in a moniliform aspect. Gap junctions between such processes can be found. Usually, the dilations are occupied by mitochondria (as revealed by Janus green B and MitoTracker Green FM) and elements of endoplasmic reticulum. Characteristically, some prolongations are flat, with a veil-like appearance, forming a labyrinthic system. ICLC display caveolae (about 1 caveola/1μm cell membrane length, or 2–4% of the relative cytoplasmic volume). Mitochondria and endoplasmic reticulum (rough and smooth) occupy 5–10% and 1–2% of cytoplasmic volume, respectively. IHC revealed positive staining for CD34, EGFR and vimentin and, only in a few cases for CD117. IHC was negative for: desmin, CD57, tau, chymase, tryptase and CD13. IF showed that ventricular ICLC expressed connexin 43. We may speculate that possible ICLC roles might be: *intercellular signaling* (neurons, myocytes, capillaries etc.) and/or *chemomechanical sensors*. For pathology, it seems attractive to think that ICLC might participate in the process of cardiac repair/remodeling, arrhythmogenesis and, eventually, sudden death.

Keywords: ventricular myocardium • interstitial cells of Cajal • Cajal-like cells • cell processes • caveolae • stromal synapses • ultrastructure • electron microscopy

Introduction

At present, the so-called interstitial cells of Cajal (ICC) are quite well described ultrastructurally and immunocytochemically [1–6]. Moreover, these ICC are implicated in rhythmicity and neural control of gastrointestinal smooth muscle [7, 8]. However, cells similar to ICC could be present outside the musculature of the gastrointestinal tract [9] and we called them interstitial

* Correspondence to: L.M. POPESCU, M.D., Ph.D.
Department of Cellular and Molecular Medicine,
"Carol Davila" University of Medicine and Pharmacy,
P.O. Box 35-29, Bucharest 35, Romania.
E-mail: LMP@jcmm.org

Cajal-like cells (ICLC). Indeed, such ICLC have been described recently in various extradigestive organs, under different denominations [10–23].

In myocardium, almost always attention was focused on working cardiac myocytes, in spite of a high connective tissue/muscular tissue ratio [24]. Until recently, there were no attempts to look for ICLC among muscular cells resident in the myocardial interstitium. However, we described in human atrial myocardial interstitium, using TEM and immunohistochemistry, a cell type similar to ICLC [25, 26]. We also reported preliminary evidence about the presence of ICLC in rat ventricular interstitium [25].

The major aim of this study was to provide extensive direct evidence on the morphological features of ICLC in rat and human ventricular myocardium and to quantitatively estimate the relationships of ventricular ICLC with contracting cells.

Material and methods

Animal tissue samples
Tissue samples were collected from male Wistar rats weighing 200–250g after animals were euthanized with an overdose of anesthetic. All rats were housed in a local facility for laboratory animal care and held, fed *ad libitum* on stock diet, according to the local ethical guidelines. This study was approved by the Bioethics Committee of the "Victor Babes" Institute of Pathology, Bucharest, according to generally accepted international standards.

Human tissue specimens
For immunohistochemistry, histologically normal portions of paraffin-embedded archived tissue, from either left or right ventricular myocardium, derived form 10 necropsy cases were used.

Thin-section microscopy (TSM)
Control semi-thin sections (less than 1 μm) were stained with 0.25% toluidine blue and examined by light microscopy (Nikon Eclipse E600). Representative photomicrographs were taken using Nikon Plan 40x and Nikon Plan Fluor 100x/1.30 oil.

Electron microscopy (TEM)
Tissue samples from both right and left ventricles were obtained and processed, as previoulsy described, for ultrastructural studies [25, 26].

In brief, tissue specimens (about 1 mm^3) were fixed in 4% glutaraldehyde (in 0.1 M cacodylate buffer), pH 7.3, for 4 h, at 4°C. After a brief wash in 0.1 M cacodylate buffer (CB), tissue samples were post-fixed with 1% osmium tetroxide in 0.1 M CB, pH 7.3, at 4°C, followed by dehydration in a graded series of ethanols. An alternative method to fix the myocardial tissue by perfusion was used too. After impregnation in propylene oxide, the samples were immersed overnight in a mixture of propylene oxide and Epon 812 resin, and embedded in Epon 812, as usually. Ultrathin sections were cut using a MT-7000 ultramicrotome (Research Manufacturing Company Inc., Tucson, AZ, USA) or a Leica ultracut UCT ultramicrotome (Leica Microsyteme Gmbh, Austria). Sections (50 nm) were collected on Formvar-coated copper grids, stained with uranyl acetate and lead citrate, and observed, at an acceleration voltage of 60 kV, in either a CM 12 Philips, a CM 301 Philips or a Leo 912 Omega electron microscope.

Stereology and morphometry
Random photomicrographs on one-micron thick sections were taken using Nikon Plan Fluor 100x/1.30 oil and used for quantitative and morphometric analysis of ICLC (*e.g.* total and relative number of cells, number and length of processes etc.). The quantitative evaluation of ICLC ultrastructural characteristics (relative volumes) was performed using the point-counting test [27]. Measurement of ICLC processes was performed on electron micrographs using NIH ImageJ software after proper calibration in Adobe Photoshop.

Immunohistochemistry
IHC was performed on formalin-fixed, human paraffin-embedded tissue sections by the avidin-biotin peroxidase complex method [28, 29]. The primary anti-
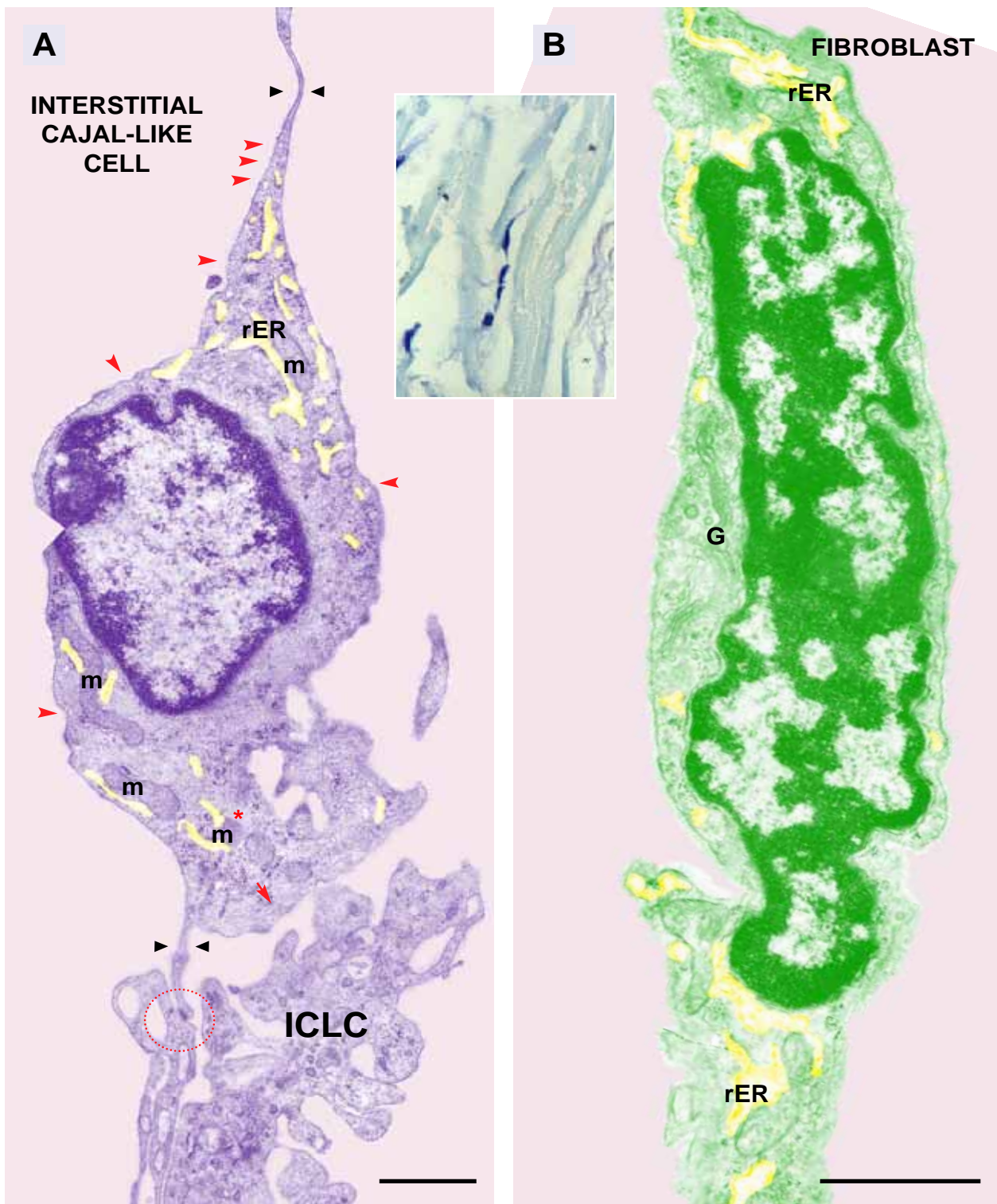
Fig. 1 A, B Digitally-colored electron micrograph of rat ventricular myocardium. **A.** Interstitial Cajal-like cell (ICLC) with a few cisternae of rough endoplasmic reticulum (rER - yellow), caveolae (arrows), intermediate filaments (*), microtubules (arrowhead) and two, 0.1μ thick, cytoplasmic processes. Note that the prolongations starting from the cell body are very thin (slender) from the very beginning (▲). This is a criterion to differentiate ICLC from fibroblasts. Note the gap junction between the ICLC and a cellular process of another ICLC (round mark). **B.** Fibroblast having indented nucleus, rER with dilated cisternae (yellow) and Golgi complexes (G). Scale bar = 1 μ. **Inset**: Light microscopy. Possible ICLC stained with toluidine blue in human ventricular myocardium (archived necroptic material).
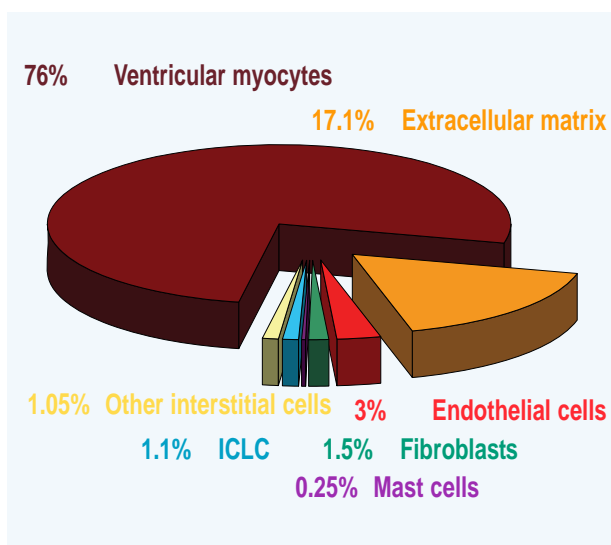
Fig. 2 Chart representing the relative volumes (%) occupied by cell populations in rat ventricular myocardium. 20 randomly taken photographs of semithin sections stained with toluidine blue were analysed.

bodies used were as follows: **CD117/c-kit**, polyclonal, 1:100 (DAKO, Glostrup, Denmark), **CD34**, monoclonal, 1: 100, clone QBEND10 (Biogenex, San Ramon, CA, USA), **EGF-R**, monoclonal, 1:1000, clone 29.1 (Sigma, St. Louis, MO, USA), **vimentin**, monoclonal, 1:100, clone V-9 (BioGenex, San Ramon, CA, USA), **smooth muscle α-actin** (SMA), monoclonal, 1:1500, clone 1A4 (Sigma Chemical, St. Louis, MO, USA), **tau** protein, polyclonal, 1:100 (NeoMarker, Fremont, CA, USA), **nestin**, monoclonal, 1:100, clone 5326 (Santa Cruz, CA, USA), **desmin**, monoclonal, 1:50, clone D33 (Dako, Glostrup, Denmark), **CD13**, monoclonal, 1:40, clone 38C12 (Novocastra, Newcastle upon Tyne, UK), **S-100**, polyclonal, 1:500 (DAKO, Glostrup, Denmark), **chymase**, monoclonal, 1:100, clone CC1 (NeoMarkers, Fremont CA) and **tryptase** monoclonal, 1:100, clone AA1 (NeoMarkers, Fremont CA) .

Immunofluorescence (IF)

Immunofluorescent staining was performed using a protocol adapted after Mora *et al.* [30]. Cells grown on coverslips were fixed using 2% paraformaldehyde for 10 minutes at room temperature, then washed in PBS and permeabilized in PBS containing 0.5% bovine serum albumine (BSA) and 0.075% saponine (PBSSA), for 15 min. Anti-connexin 43 primary antibodies (1:50, clone H150, Santa Cruz CA, USA) were applied for 1 h, at room temperature. Polyclonal FITC-labeled goat anti-mouse antibodies (working dilution 1:100, BD Pharmingen, San Jose, CA, USA) were used to detect the primary immune reaction. Finally, nuclei were counterstained with 1 µg/ml Hoechst 33342 (Sigma Chemical, St. Louis, MO, USA), and samples examined under a Nikon TE300 microscope equipped with a Nikon DX1 camera, Nikon PlanApo 40x and 60x objectives, and the appropriate fluorescence filters. Negative controls were prepared following the same protocol, but omitting the primary antibodies.

Ventricular interstitial-cell isolation protocol

Male Wistar rat (4 weeks) was killed by cervical dislocation. Hearts were removed and immediately placed in Dulbecco's Modified Eagle's Medium (DMEM), then disected and repeatedly washed with DMEM supplemented with 100 UI/ml penicillin, 0.1 mg/ml streptomycin, and 0.25 µg/ml amphotericin (Sigma Chemical, St.Louis, MO, USA). After mechanical removal of pericardium and endocardium, the remaining ventricular tissue was minced in fragments of about 1 mm^3, rinsed and incubated on an orbital shaker for 30 min, at 37°C, with 1.5 mg/ml collagenase type Ia (Sigma Chemical, St.Louis, MO, USA) in PBS. Dispersed cells were separated from non-digested tissue by filtration through a 40 µm diameter cell strainer (BD Labware, San Jose, CA, USA), collected by centrifugation at 250g, and resuspended in a 1:1 DMEM:Ham's Nutrient F-12 mixture, supplemented with 10% fetal calf serum, 1.5 mM HEPES, 100 UI/ml penicillin, 0.1 mg/ml streptomycin and 0.25 µg/ml amphotericin. Cell density was counted in a haemocytometer and viability was assessed using the Trypan blue exclusion test. Cells were distributed on glass coverslips into 24-well plates (BD Labware, San Jose,CA, USA) at a density of 1.5x10^4 cells/cm^2, and maintained at 37°C, in a humidified atmosphere (5% CO_2 in air) until becoming semi-confluent (usually 4 days after plating).
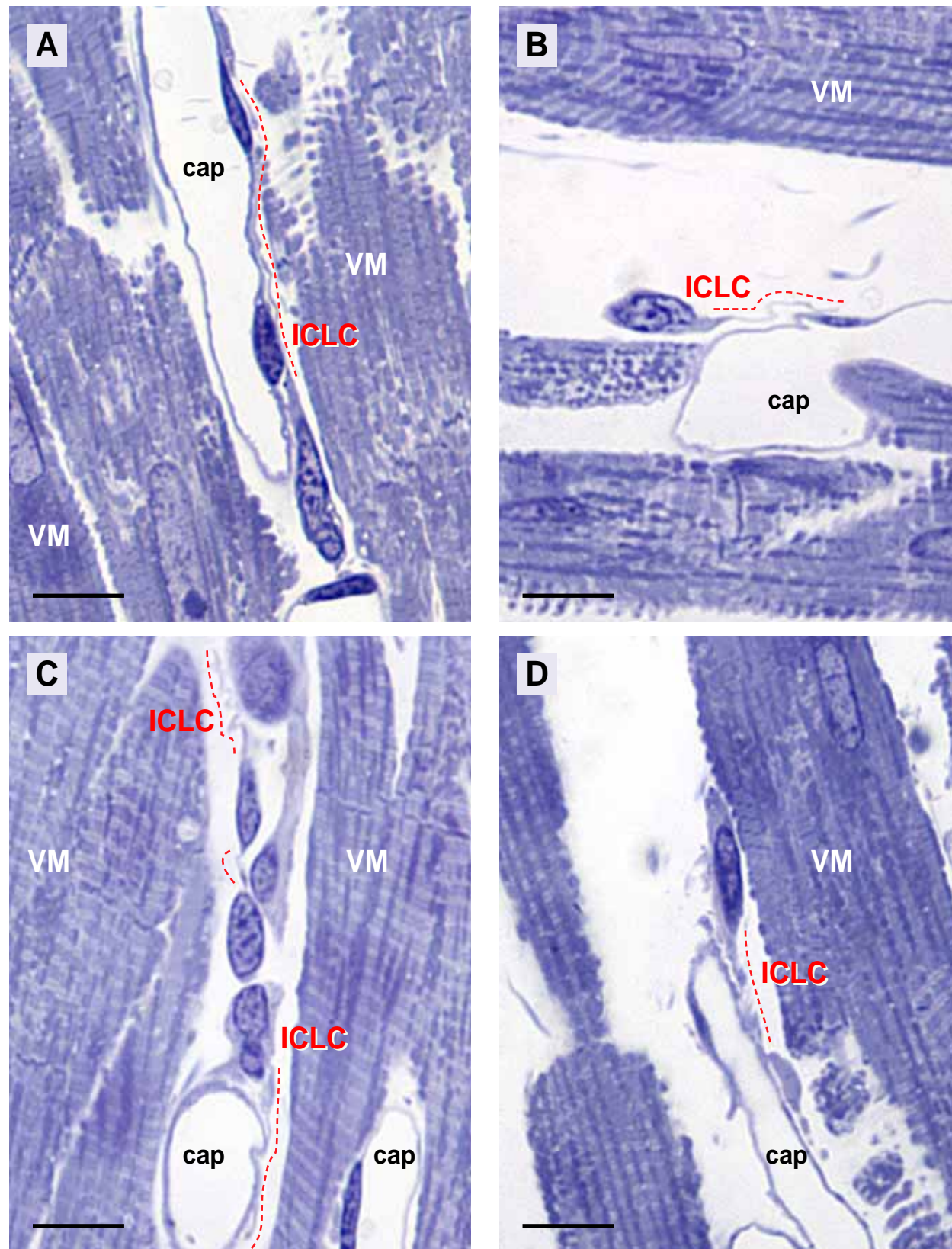
Fig. 3 A–F   Rat ventricular myocardium. Toluidine blue stained ICLC among working cardiomyocytes and capillaries. Long, ICLC thin processes, delineated by red dotted lines, in close vicinity with capillaries. cap = capillary, VM = ventricular myocyte. Scale bars = 10μm.
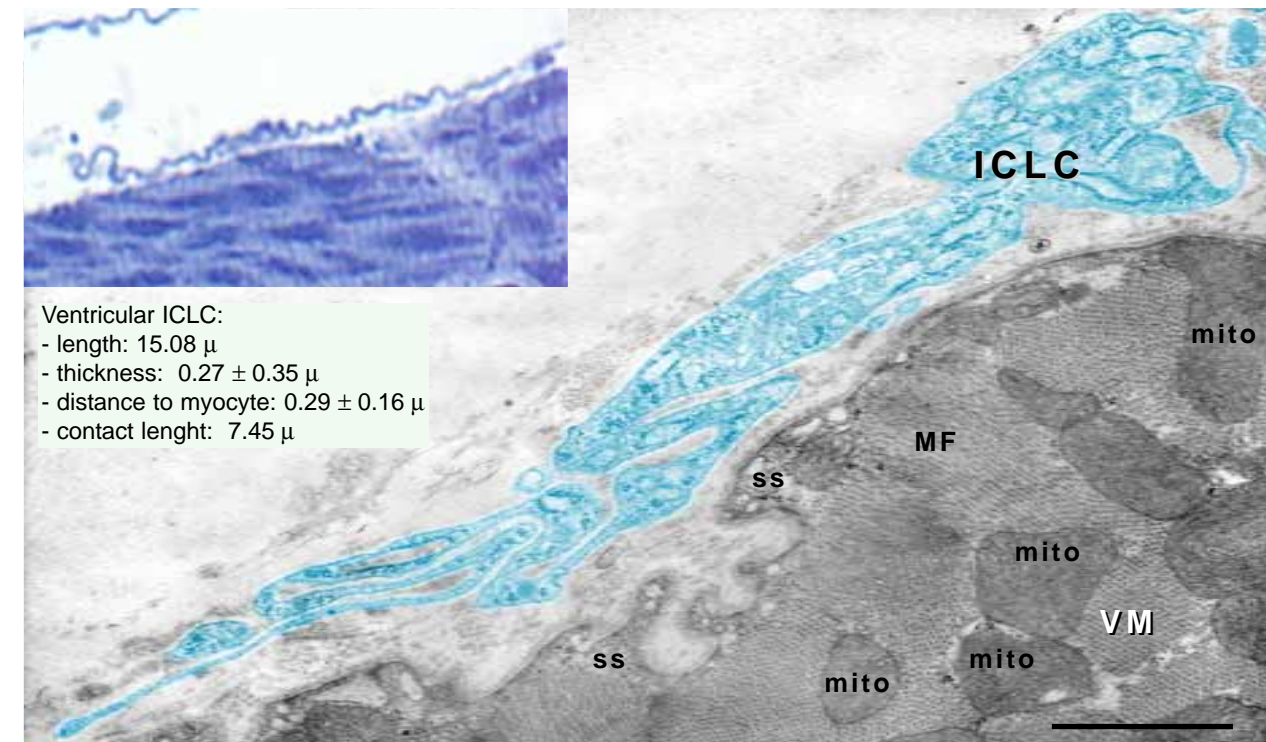

Ventricular ICLC:
- length: 15.08 μ
- thickness: 0.27 ± 0.35 μ
- distance to myocyte: 0.29 ± 0.16 μ
- contact lenght: 7.45 μ

Fig. 4   ICLC extensions (ICLC) with a typical labyrinthine feature in apposition with the basal lamina of a ventricular myocyte (VM). mito = mitochondria; VM = ventricular myocyte; MF = myofilaments; ss = subsarcolemmal vesicles. Scale bar = 1 μm.
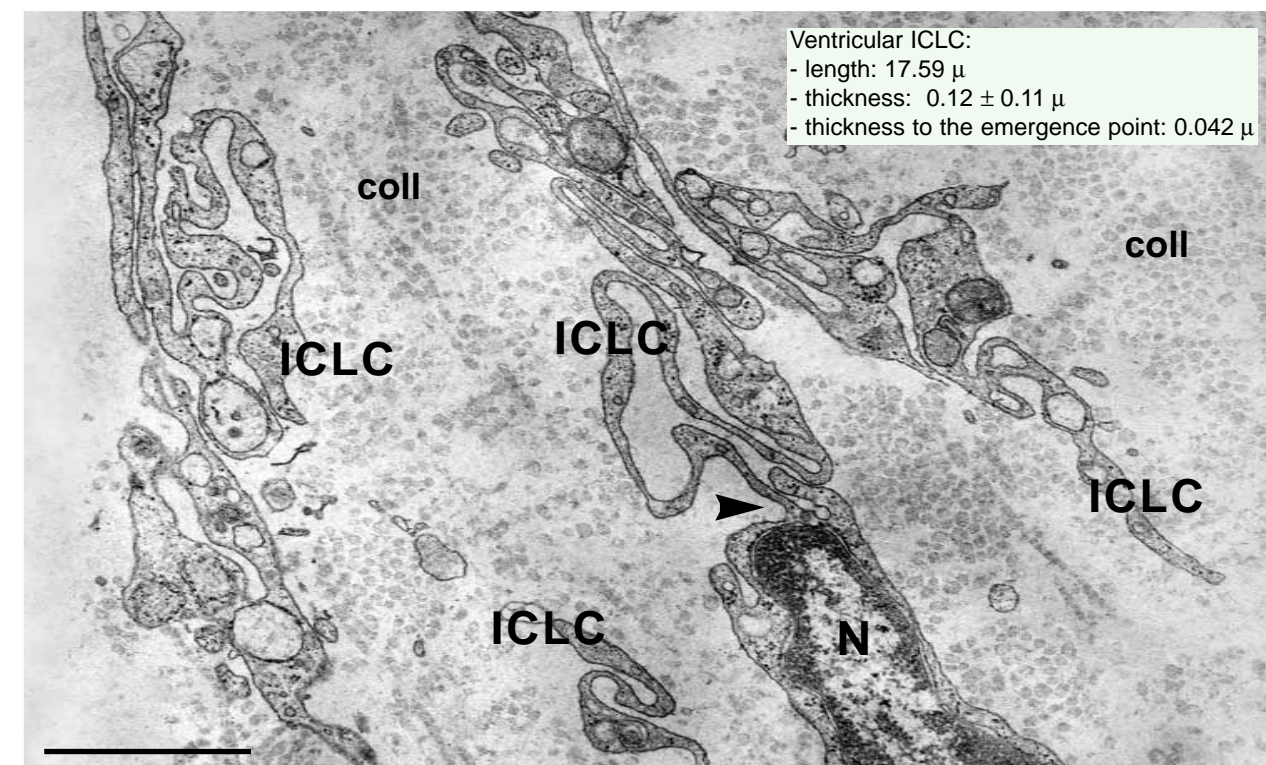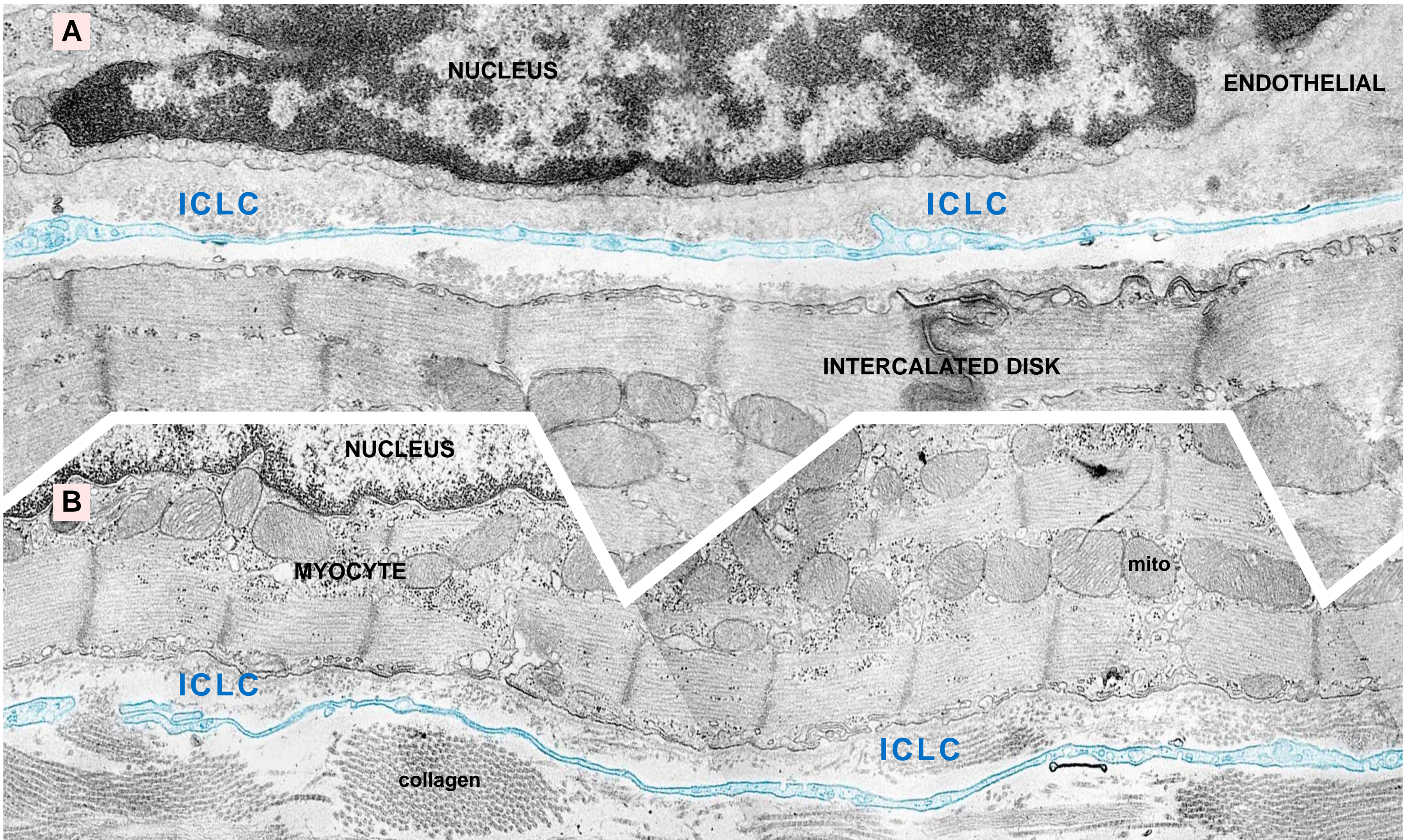

Ventricular ICLC:
- length: 17.59 μ
- thickness: 0.12 ± 0.11 μ
- thickness to the emergence point: 0.042 μ

Fig. 5   Several retracted veil-like cytoplasmic extensions belonging to ICLC, containing free ribosomes, a few mitochondria, caveolae and enlarged sER. Note that the cytoplamic processes are slender at their emergence point (arrowhead). The cells are placed in a collagen fibers meshwork. coll = collagen; N = nucleus. Scale bar = 1 μm.
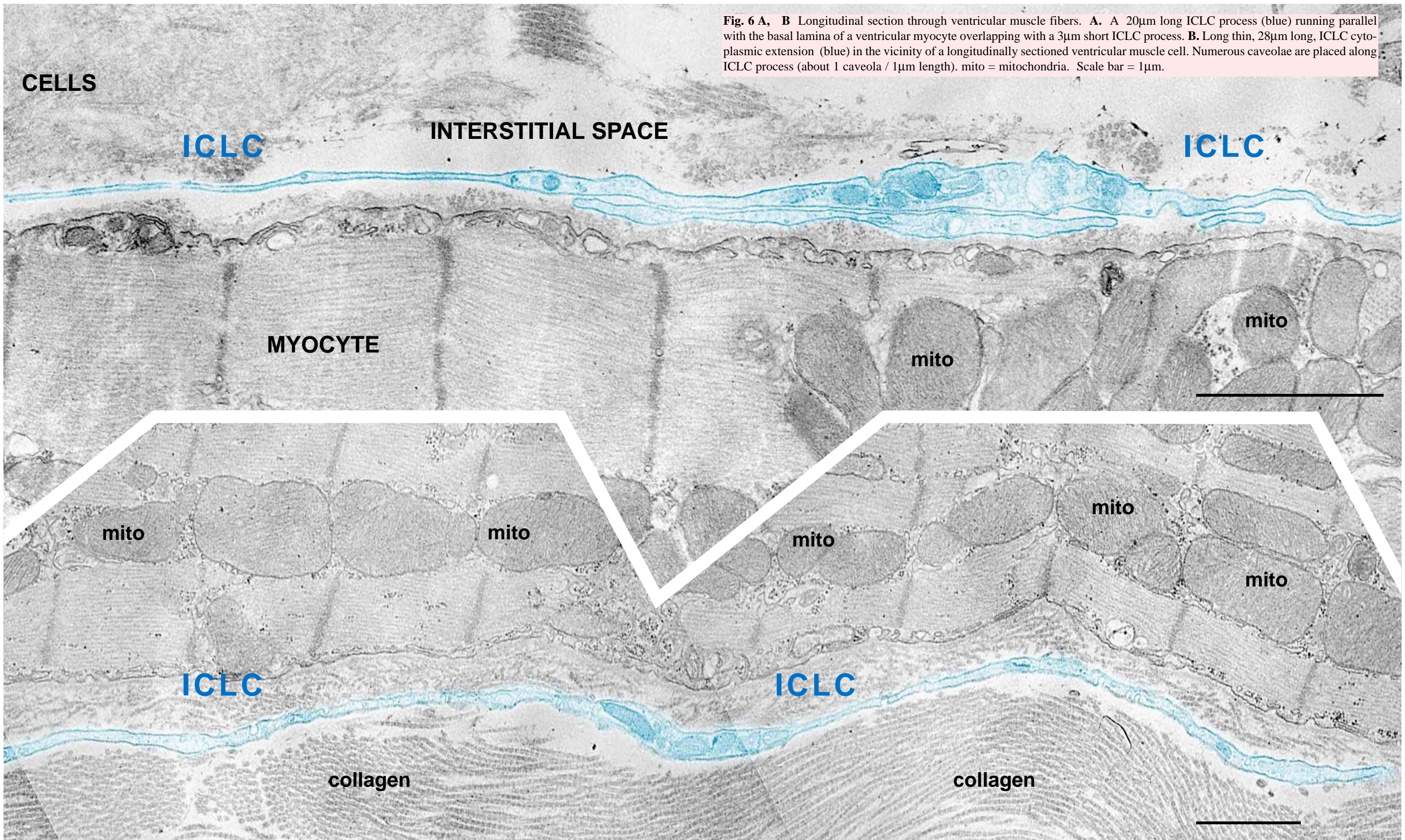
A

NUCLEUS

ENDOTHELIAL

ICLC   ICLC

INTERCALATED DISK

NUCLEUS

B

MYOCYTE   mito

ICLC

ICLC

collagen

434

Fig. 6 A, B Longitudinal section through ventricular muscle fibers. **A.** A 20µm long ICLC process (blue) running parallel with the basal lamina of a ventricular myocyte overlapping with a 3µm short ICLC process. **B.** Long thin, 28µm long, ICLC cytoplasmic extension (blue) in the vicinity of a longitudinally sectioned ventricular muscle cell. Numerous caveolae are placed along ICLC process (about 1 caveola / 1µm length). mito = mitochondria. Scale bar = 1µm.

Ventricular ICLC:
- length: 19.06 μm
- thickness: 0.20 ± 0.11 μm
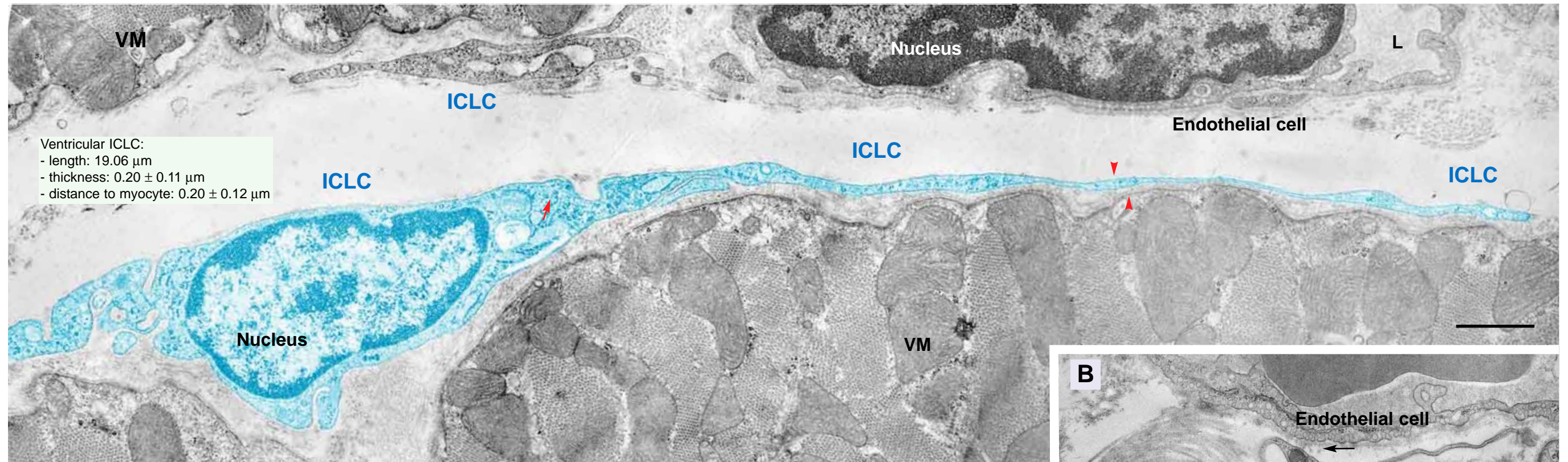- distance to myocyte: 0.20 ± 0.12 μm

Fig. 7 Cross section through ventricular muscle cells. A bipolar ICLC with cellular processes containing caveolae (arrowhead), microtubules (arrows) and few rER cisternae. The long and μ thick citoplasmic process lies on the basal lamina of the ventricular myocyte. VM - ventricular myocyte; End. - endothelial cell, L - capillary lumen. Scale bar = 1 μm.
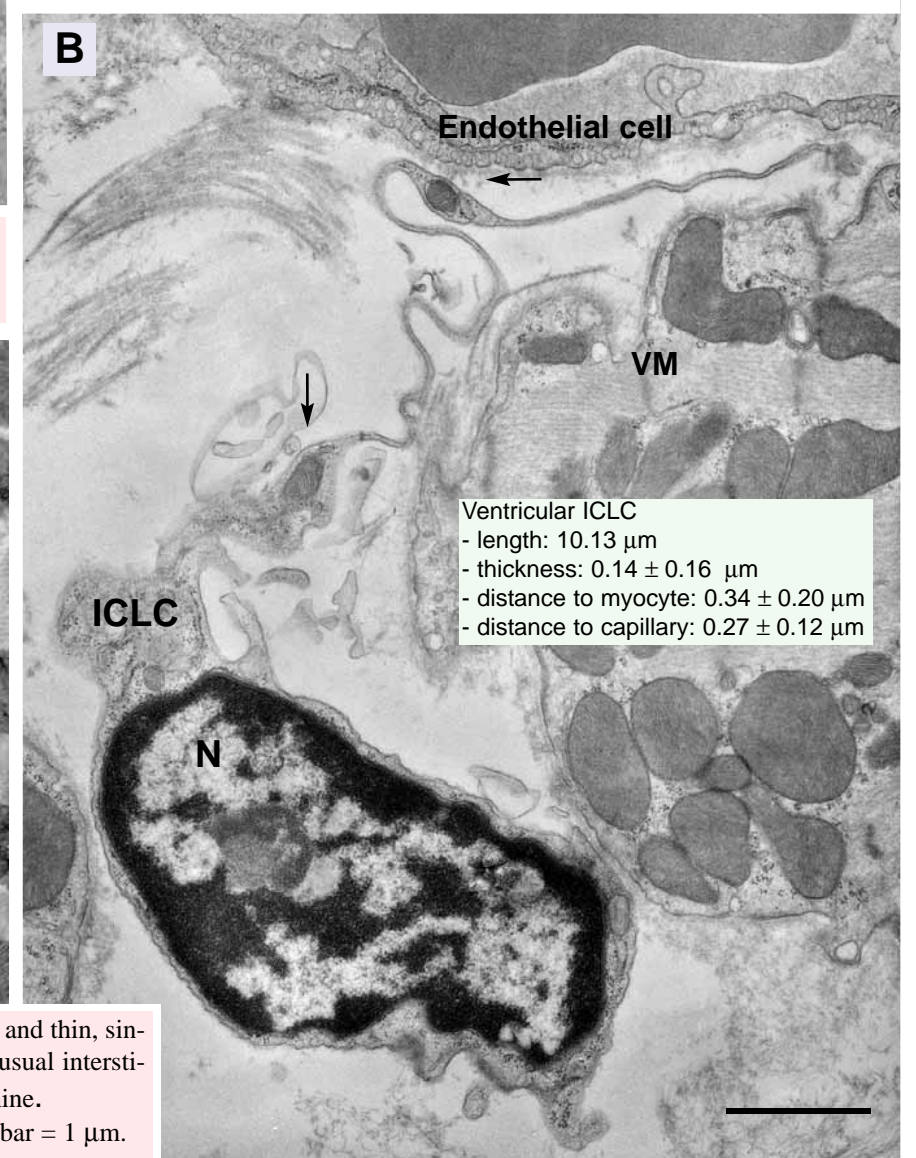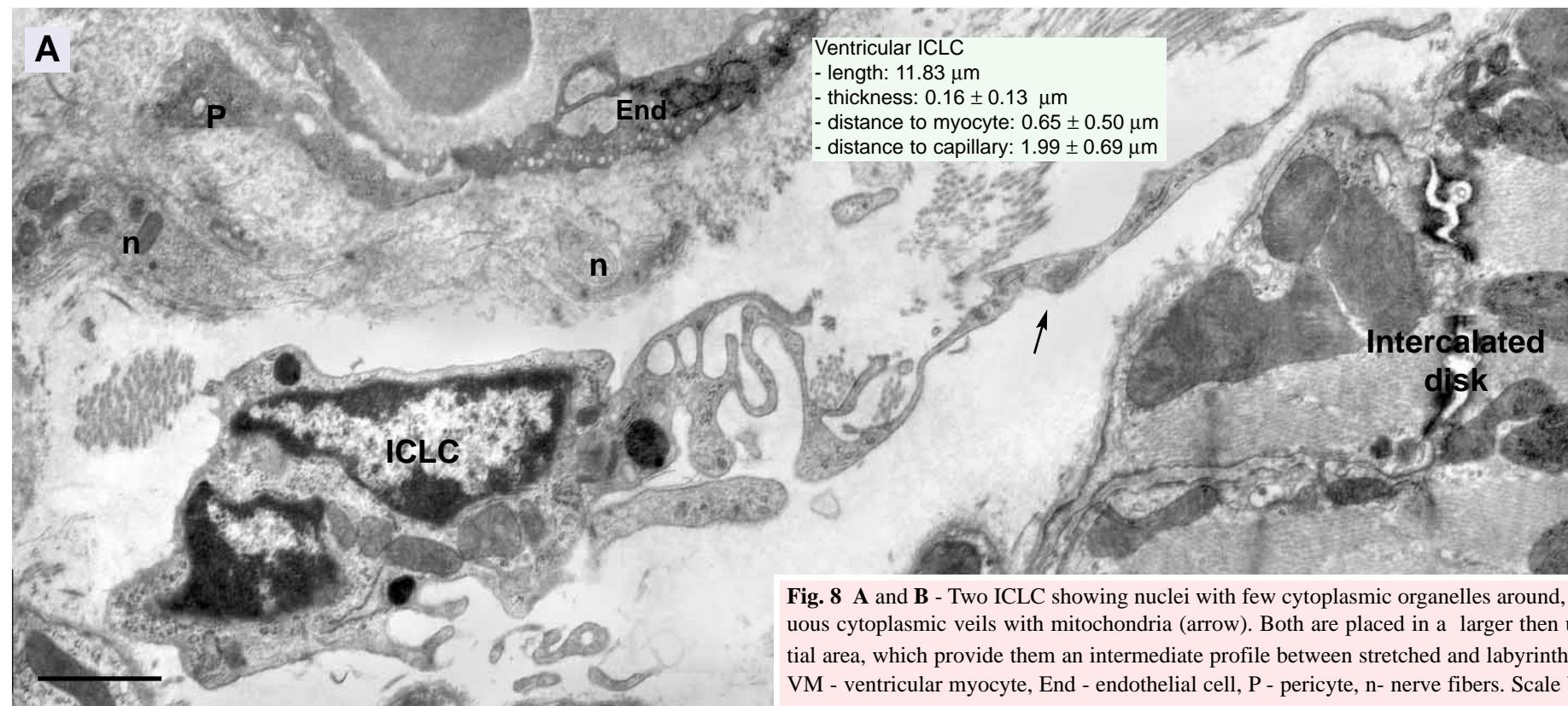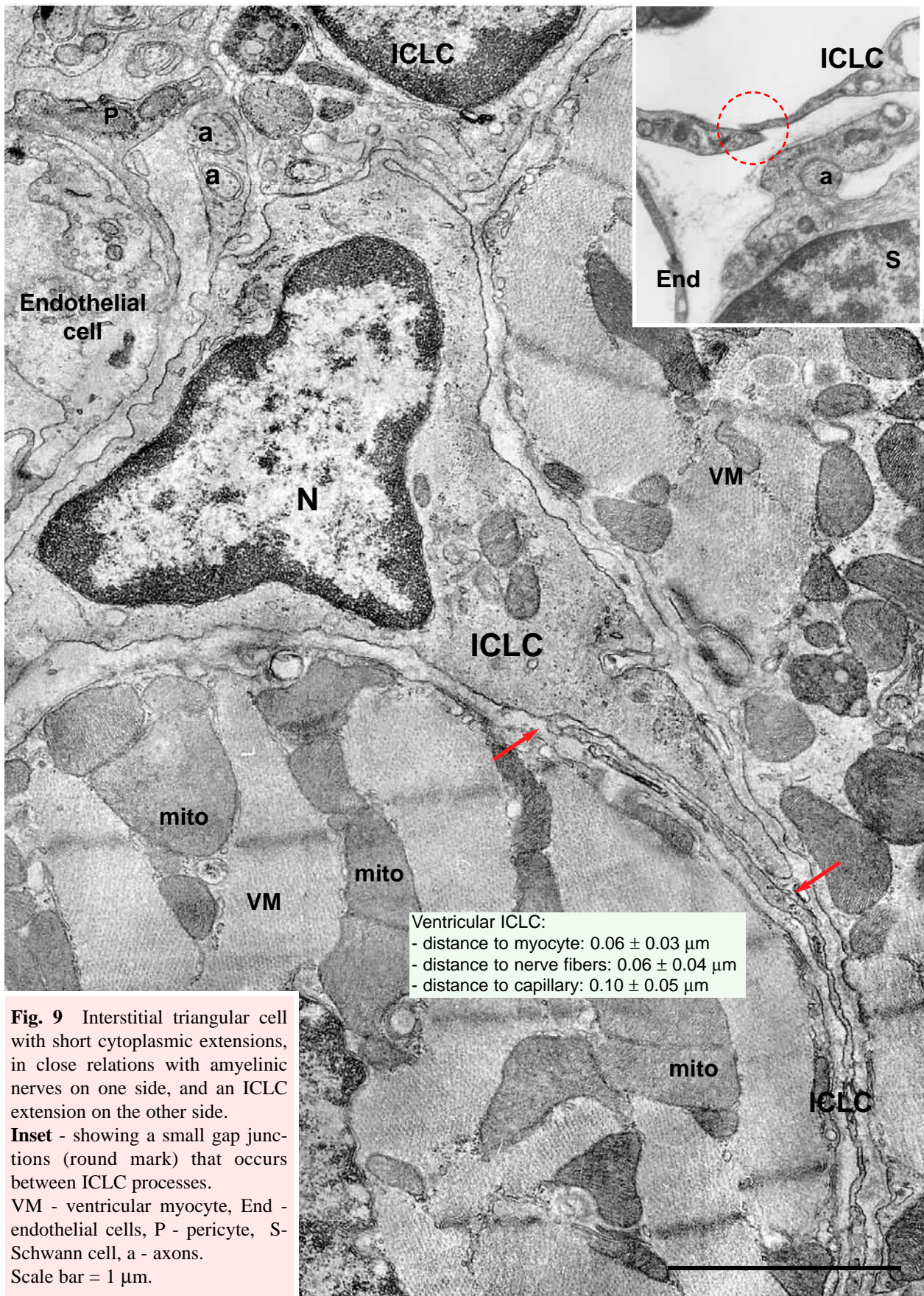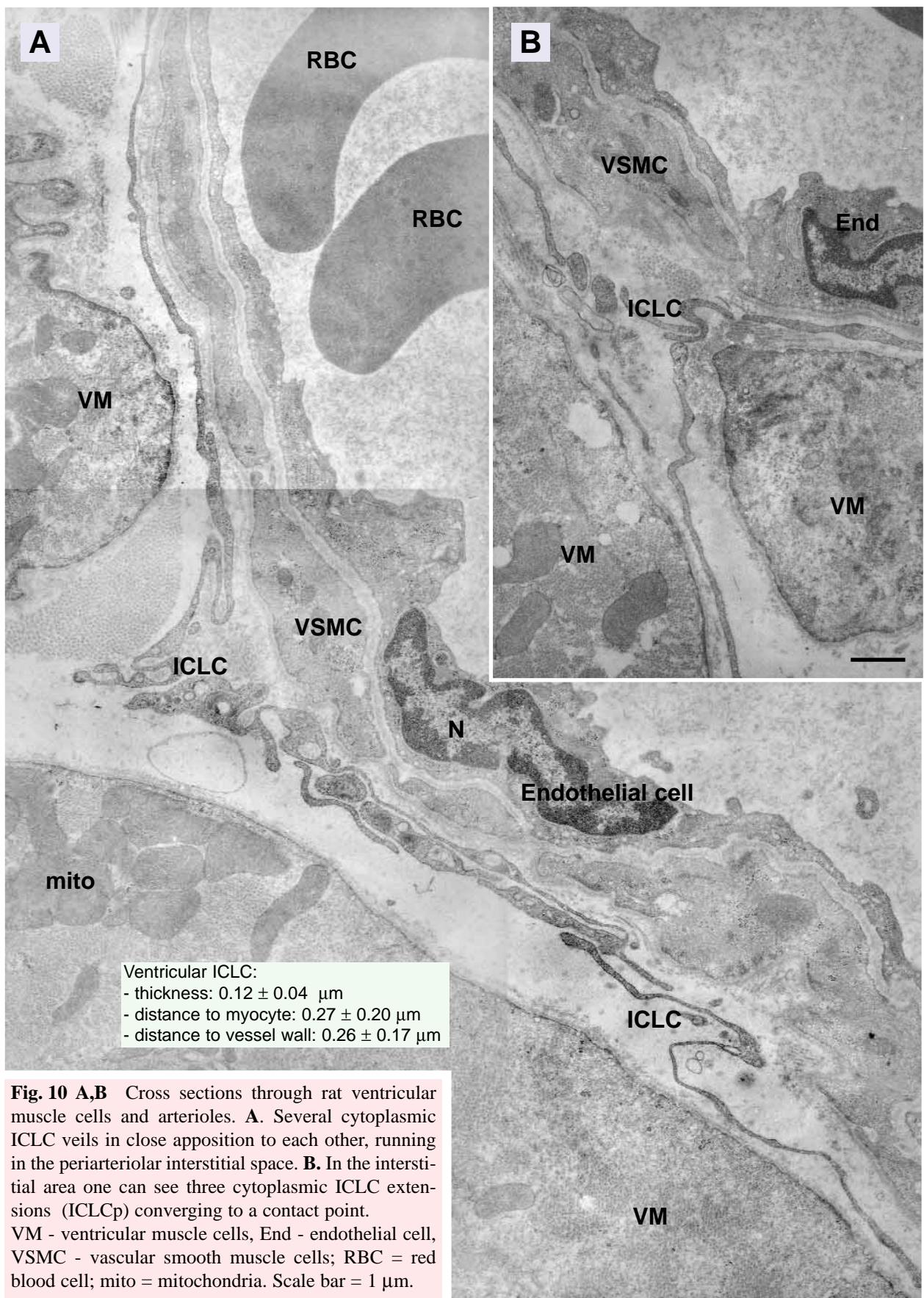

Ventricular ICLC
- length: 11.83 μm
- thickness: 0.16 ± 0.13 μm
- distance to myocyte: 0.65 ± 0.50 μm
- distance to capillary: 1.99 ± 0.69 μm

Ventricular ICLC
- length: 10.13 μm
- thickness: 0.14 ± 0.16 μm
- distance to myocyte: 0.34 ± 0.20 μm
- distance to capillary: 0.27 ± 0.12 μm

Fig. 8 A and **B** - Two ICLC showing nuclei with few cytoplasmic organelles around, and thin, sinuous cytoplasmic veils with mitochondria (arrow). Both are placed in a larger then usual interstitial area, which provide them an intermediate profile between stretched and labyrinthine.
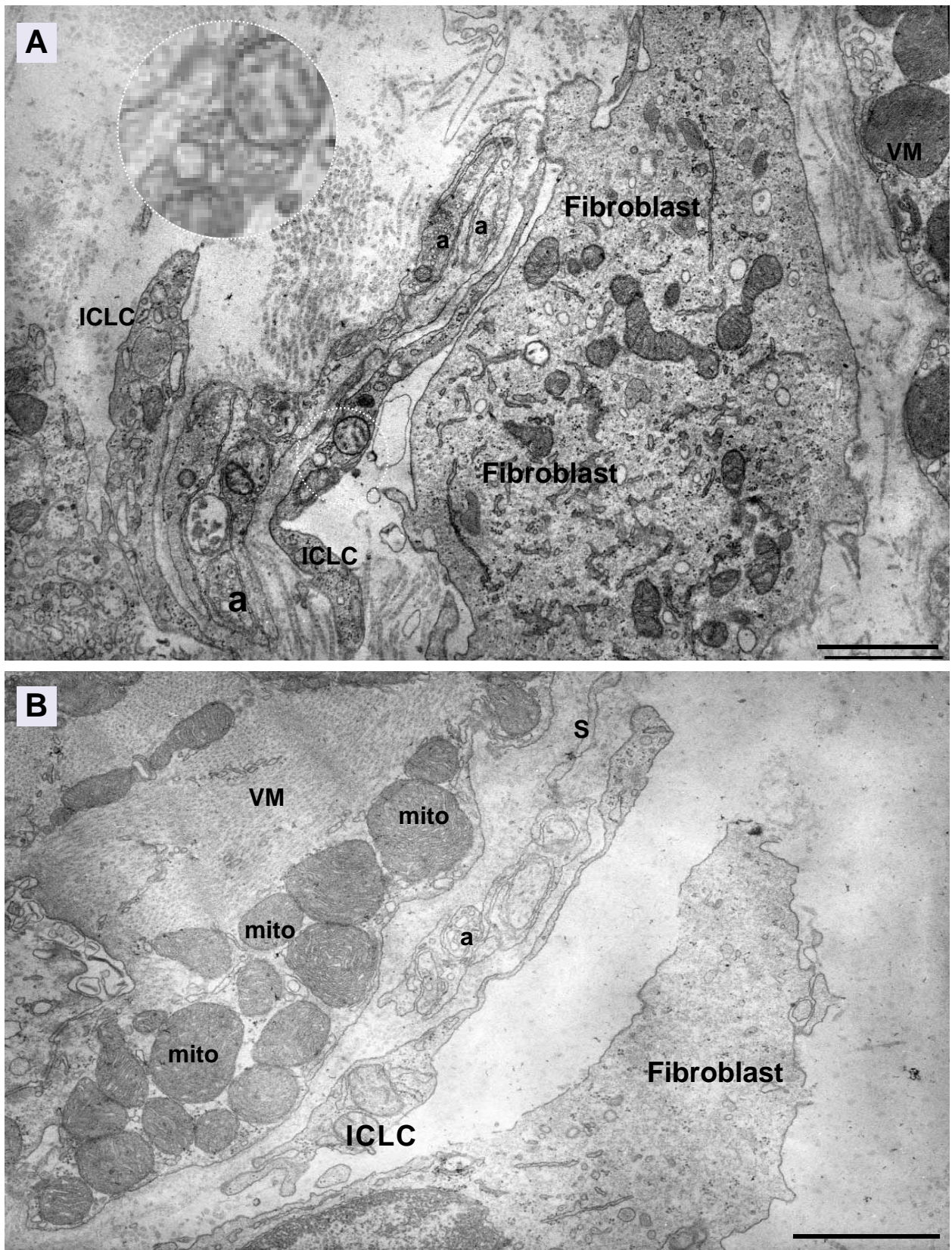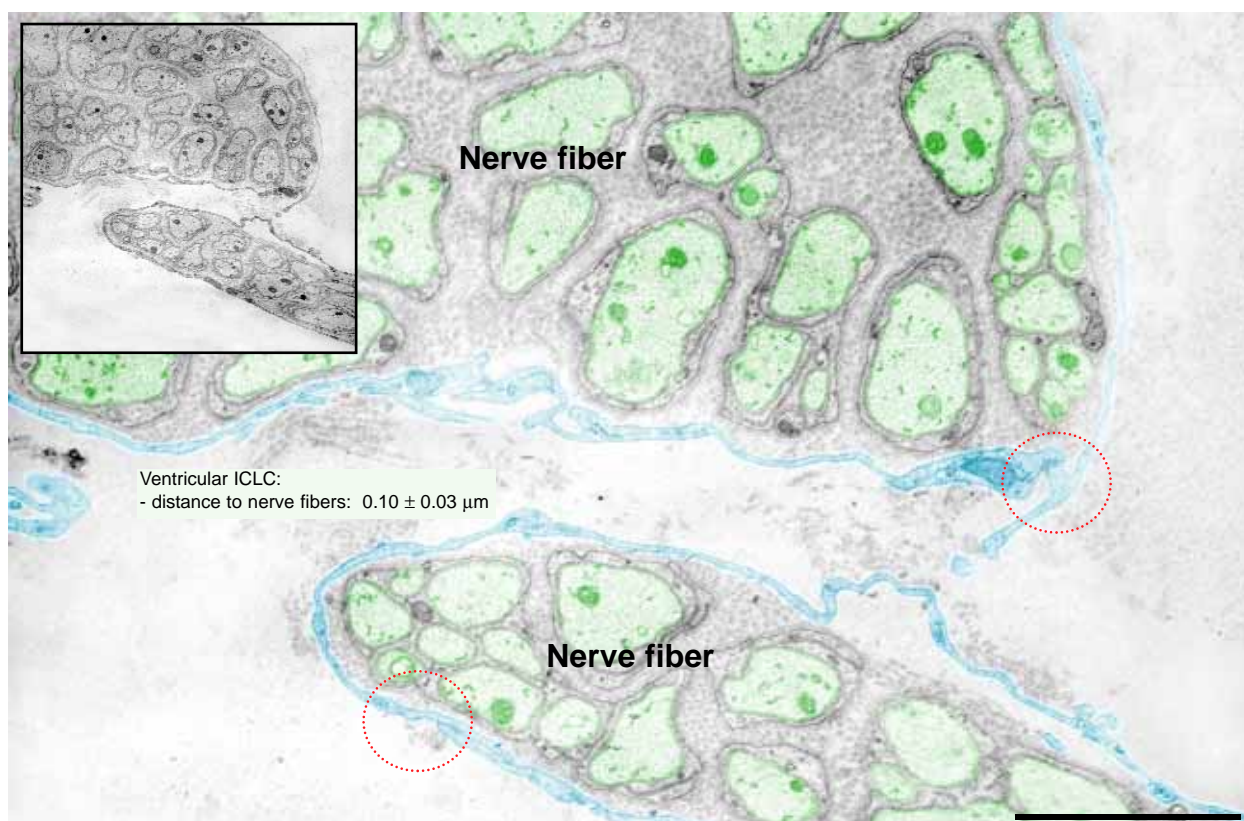VM - ventricular myocyte, End - endothelial cell, P - pericyte, n- nerve fibers. Scale bar = 1 μm.

436

Fig. 9 Interstitial triangular cell with short cytoplasmic extensions, in close relations with amyelinic nerves on one side, and an ICLC extension on the other side.
Inset - showing a small gap junctions (round mark) that occurs between ICLC processes.
VM - ventricular myocyte, End - endothelial cells, P - pericyte, S- Schwann cell, a - axons.
Scale bar = 1 μm.

Ventricular ICLC:
- distance to myocyte: 0.06 ± 0.03 μm
- distance to nerve fibers: 0.06 ± 0.04 μm
- distance to capillary: 0.10 ± 0.05 μm

A

RBC

RBC

VM

VSMC

ICLC

N

mito

Ventricular ICLC:
- thickness: 0.12 ± 0.04 μm
- distance to myocyte: 0.27 ± 0.20 μm
- distance to vessel wall: 0.26 ± 0.17 μm

B

VSMC

End

ICLC

VM

VM

Endothelial cell

ICLC

VM

Fig. 10 A,B Cross sections through rat ventricular muscle cells and arterioles. **A.** Several cytoplasmic ICLC veils in close apposition to each other, running in the periarteriolar interstitial space. **B.** In the interstitial area one can see three cytoplasmic ICLC extensions (ICLCp) converging to a contact point.
VM - ventricular muscle cells, End - endothelial cell, VSMC - vascular smooth muscle cells; RBC = red blood cell; mito = mitochondria. Scale bar = 1 μm.

438

Fig. 11 A.B. - Close proximity of ventricular muscle cell (M), unmyelinated axons (a), ICLC processes (ICLC) and fibroblast (F), S - Schwan cell. Scale bar = 1 μm.

Fig.12 Digitally-colored electron micrograph. Large unmyelinated nerves (green - axons) placed in the interstitium between muscle cells. The nerve fibers are surrounded by slender cytoplasmic extensions of the ICLC (blue). Note the gap junctions (round mark) between ICLC processes. Scale bar = 1 μm. Inset - genuine photomicrograph.

Silver impregnation on cell cultures was done as follows: cells were fixed with paraformaldehyde 2% for 10 min, at 4ºC, washed 3 times in ethanol 80% and then incubated with silver nitrate 20%, for 30 min. Coverslips were then washed 3 times with water and covered with paraformaldehyde 20% for 3 min and then with amoniacal silver nitrate solution for 30 sec. Slides were then washed in distilled water, fixed in thiosulphate 5% and mounted in Entellan (Merck KGaA, Darmstadt, Germany).

Vital stainings

Methylene blue vital staining. Cells were washed in prewarmed phenol red-free DMEM (Sigma Chemical, St. Louis, MO, USA), and incubated for 20 min, in a 0.02% methylene-blue solution, at 37ºC. Methylene-blue solutions with dilutions between 0.01–0.1% have

been tested and 0.02% was chosen as being optimal. Cells were examined and photographed under a Nikon inverted TE200 microscope equipped with a Nikon DN-5 digital camera.

Janus green B vital staining. Cells in culture were stained for 30 min in 0.02% Janus green B (Sigma Chemical, St. Louis, MO, USA) in DMEM and maintained at 37°C, in a humidified atmosphere, 5% CO_2 in air. After repeated washes in DMEM, cells were examined under a heated object stage inverted Nikon TE200 microscope and photographed.

Giemsa staining. The 35 mm Petri culture-dishes were emptied of the culture medium and cells were stained with 0.4% Giemsa solution (Sigma Chemical, St. Louis, MO, USA) in methanol and distilled water (pH 6.9), for 30 min, at room temperature.This method is not a vital one, since the dye and the fixation agent
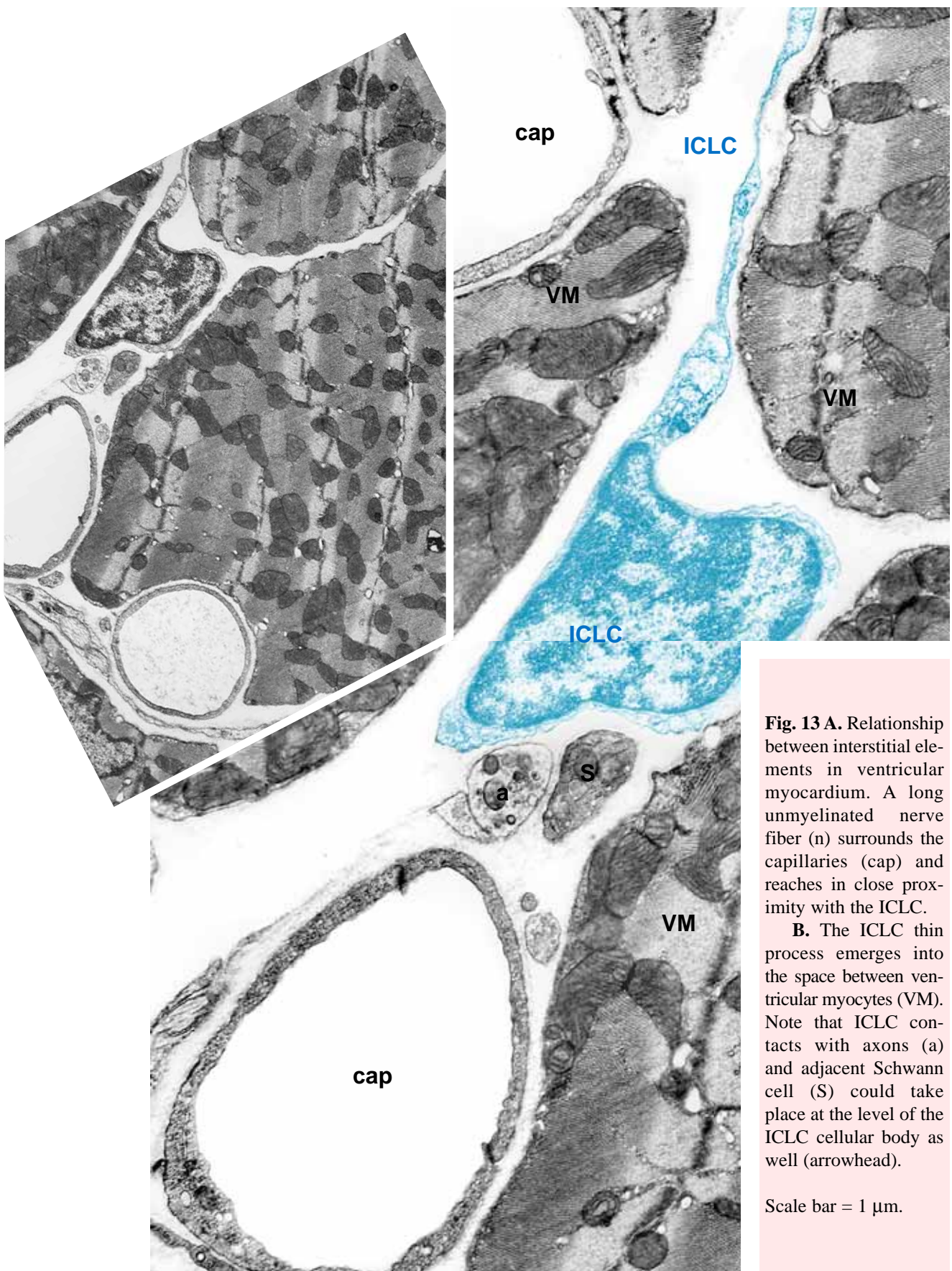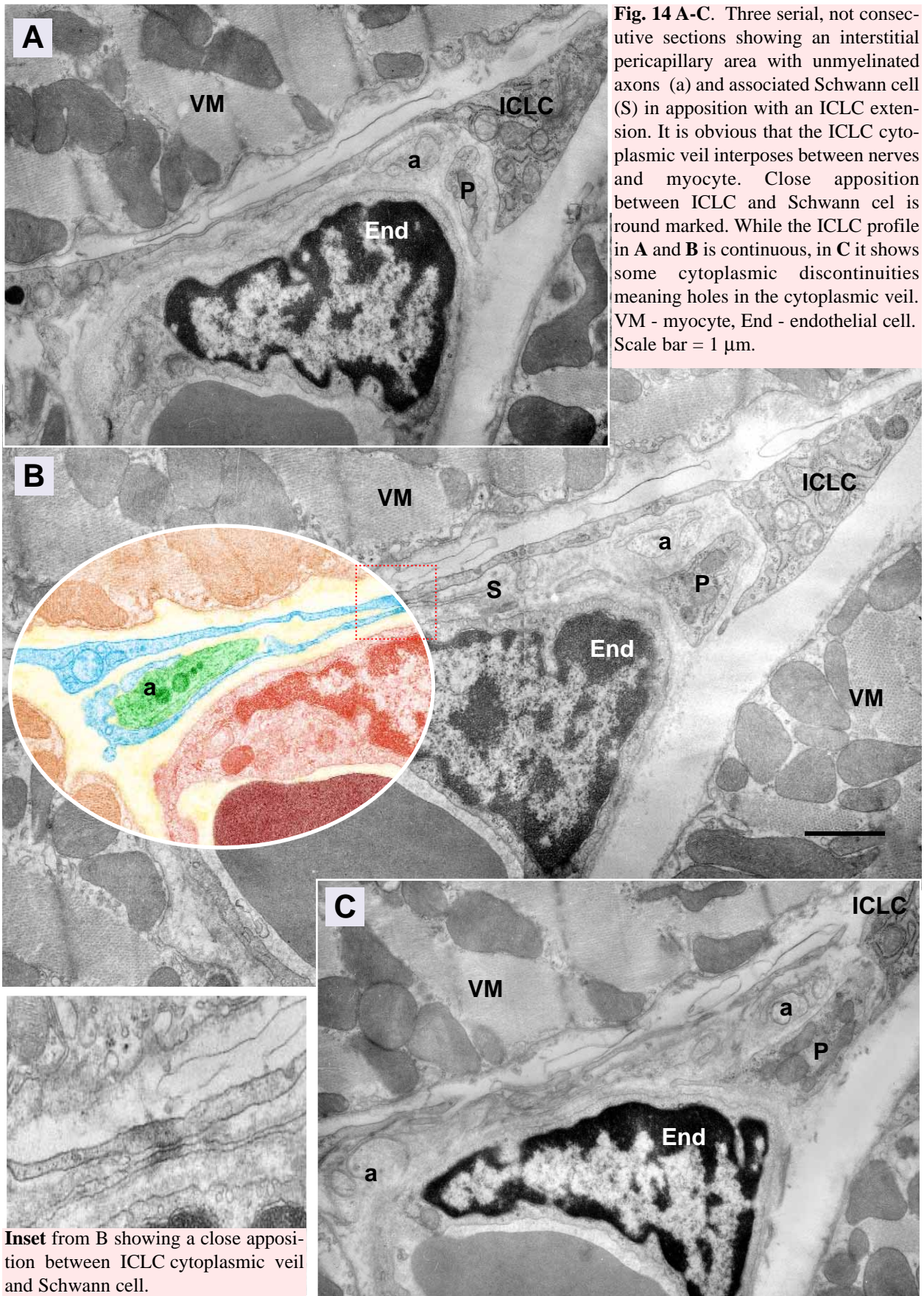
440

Fig. 13 A. Relationship between interstitial elements in ventricular myocardium. A long unmyelinated nerve fiber (n) surrounds the capillaries (cap) and reaches in close proximity with the ICLC.

B. The ICLC thin process emerges into the space between ventricular myocytes (VM). Note that ICLC contacts with axons (a) and adjacent Schwann cell (S) could take place at the level of the ICLC cellular body as well (arrowhead).
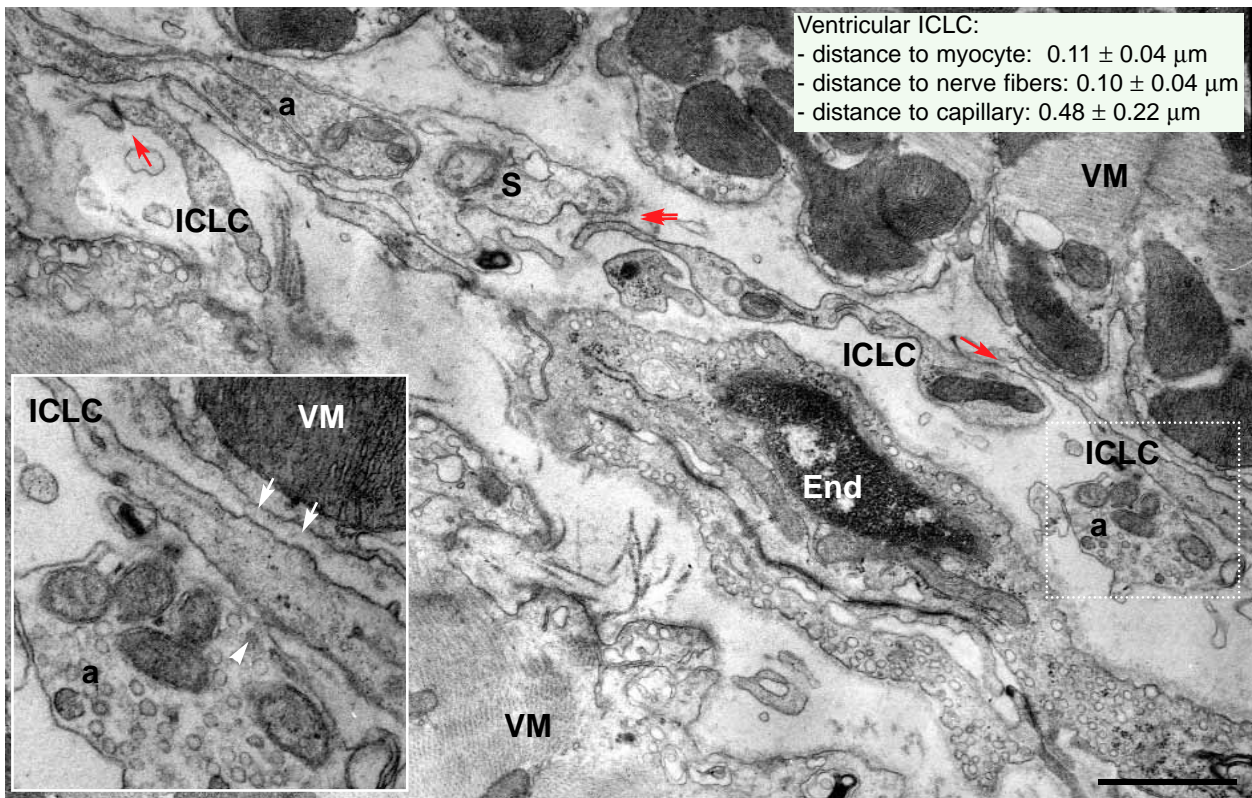
Scale bar = 1 μm.

Fig. 14 A-C. Three serial, not consecutive sections showing an interstitial pericapillary area with unmyelinated axons (a) and associated Schwann cell (S) in apposition with an ICLC extension. It is obvious that the ICLC cytoplasmic veil interposes between nerves and myocyte. Close apposition between ICLC and Schwann cel is round marked. While the ICLC profile in **A** and **B** is continuous, in **C** it shows some cytoplasmic discontinuities meaning holes in the cytoplasmic veil. VM - myocyte, End - endothelial cell. Scale bar = 1 μm.

Inset from B showing a close apposition between ICLC cytoplasmic veil and Schwann cell.

442

Ventricular ICLC:
- distance to myocyte: 0.11 ± 0.04 μm
- distance to nerve fibers: 0.10 ± 0.04 μm
- distance to capillary: 0.48 ± 0.22 μm

Fig. 15 - Interstitial pericapillary area. Unmyelinated axons (a) and associated Schwann cell (S) in close apposition (double arrow) with an ICLC process. The ICLC processes have gap junctions (arrows). Details in **inset**: a point contact with a terminal axon filled with synaptic vesicles (arrowhead); the distance between ICLC and cardiomyocyte (VM) is 30±5 nm (arrows). End - endothelial cell. Scale bar = 1 μm.
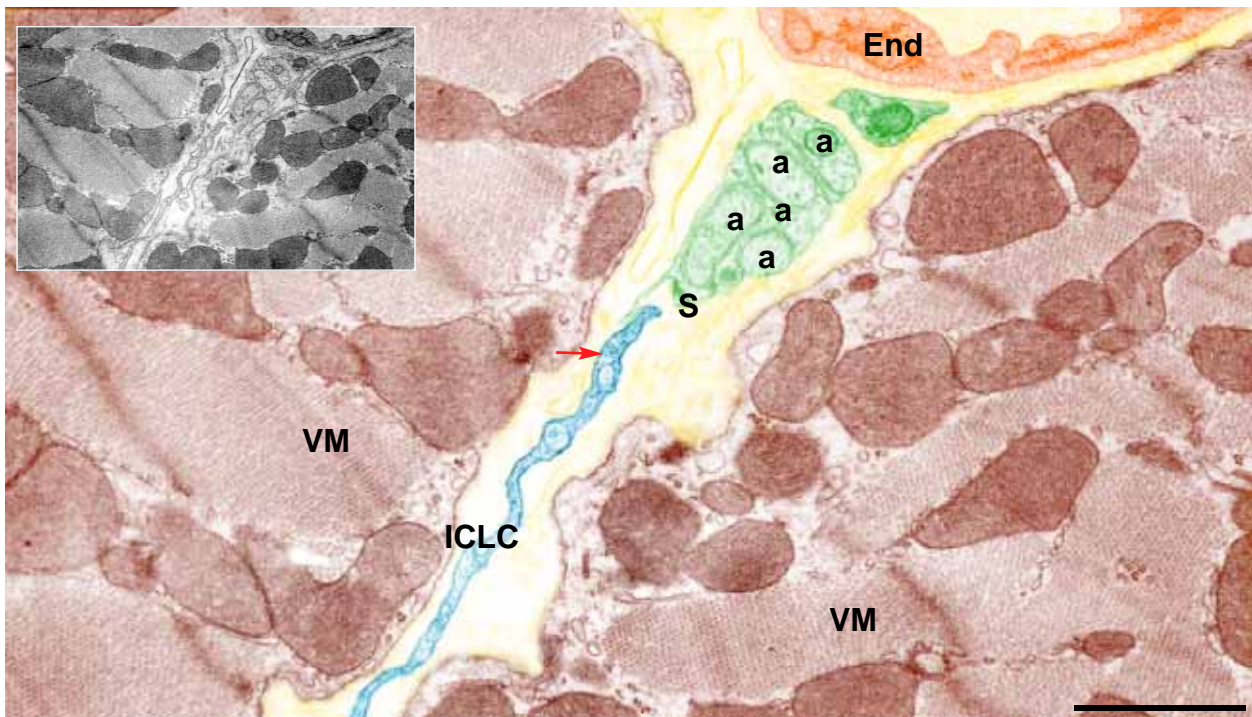
Fig. 16 - Interstitial ventricular space containing two myocytes (VM), a blood capillary (End), axons (a) and associated Schwann cell (S), an ICLC process and a small junctional area in between (arrow). Scale bar = 1 μm
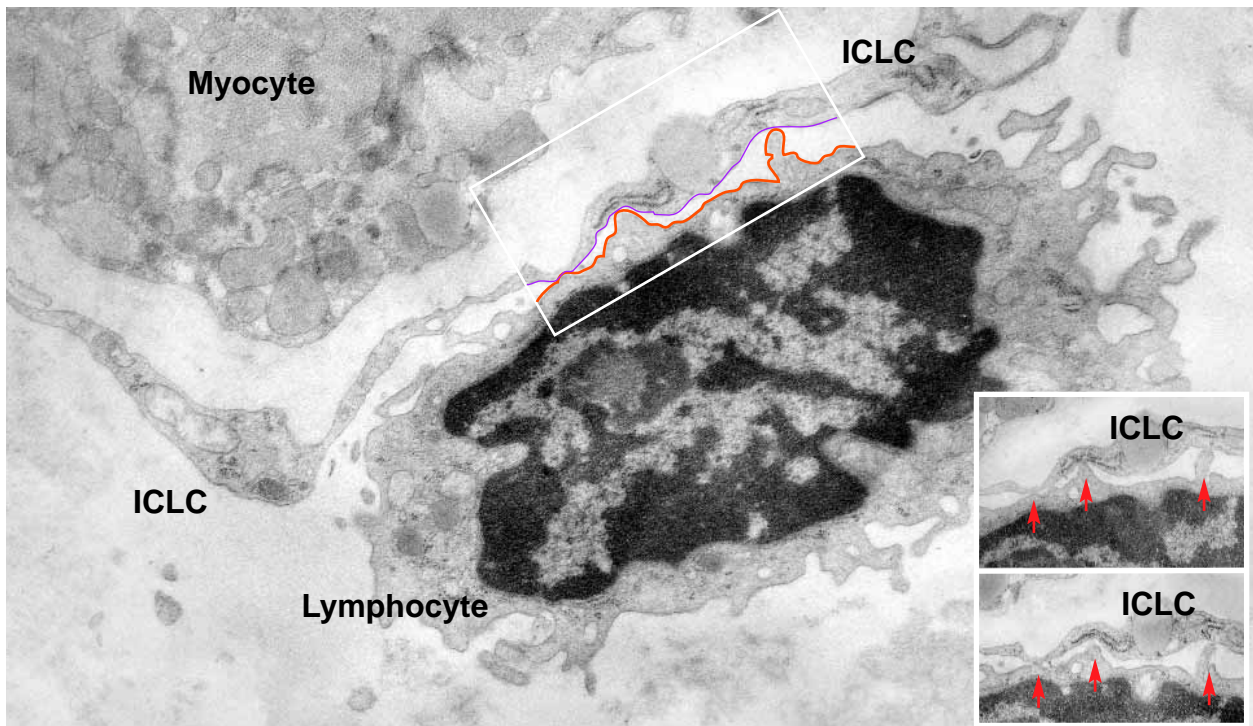
Fig. 17 Lymphocyte-ICLC multicontact stromal synapse. The ICLC process is interposed between a myocyte (VM) and a lymphocyte. Scale bar = 1 μm. **Inset**- Details of the stromal synapse on two serial sections with 0.2 μ in between showing several point contacts.
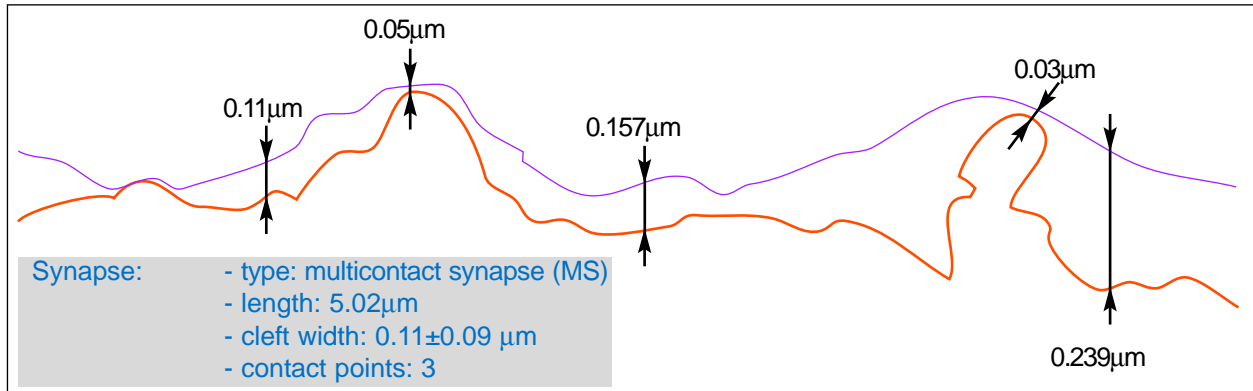
(methanol) are acting concomitantly on live cells. Cells were washed three times in distilled water and examined.

Mitochondria labeling with MitoTracker Green FM Cultures were labeled with MitoTracker Green FM (Molecular Probes, Eugene, OR, USA), the lipophylic, selective dye, which is concentrated by active mitochondria [31, 32]. Cells grown on coverslips were removed from culture and incubated in phenol red-free DMEM completed with 10% fetal calf serum and antibiotic-antimycotic solution (Sigma Chemical, St. Louis, MO, USA) in the presence of 80nM MitoTracker Green FM. Cells were incubated for 30 min, at 37°C, in a humidified atmosphere (5% CO_2 in air), subsequently washed, and examined by fluorescence microscopy (450-490 nm excitation light, 520 nm barrier filter; Nikon TE200 microscope).
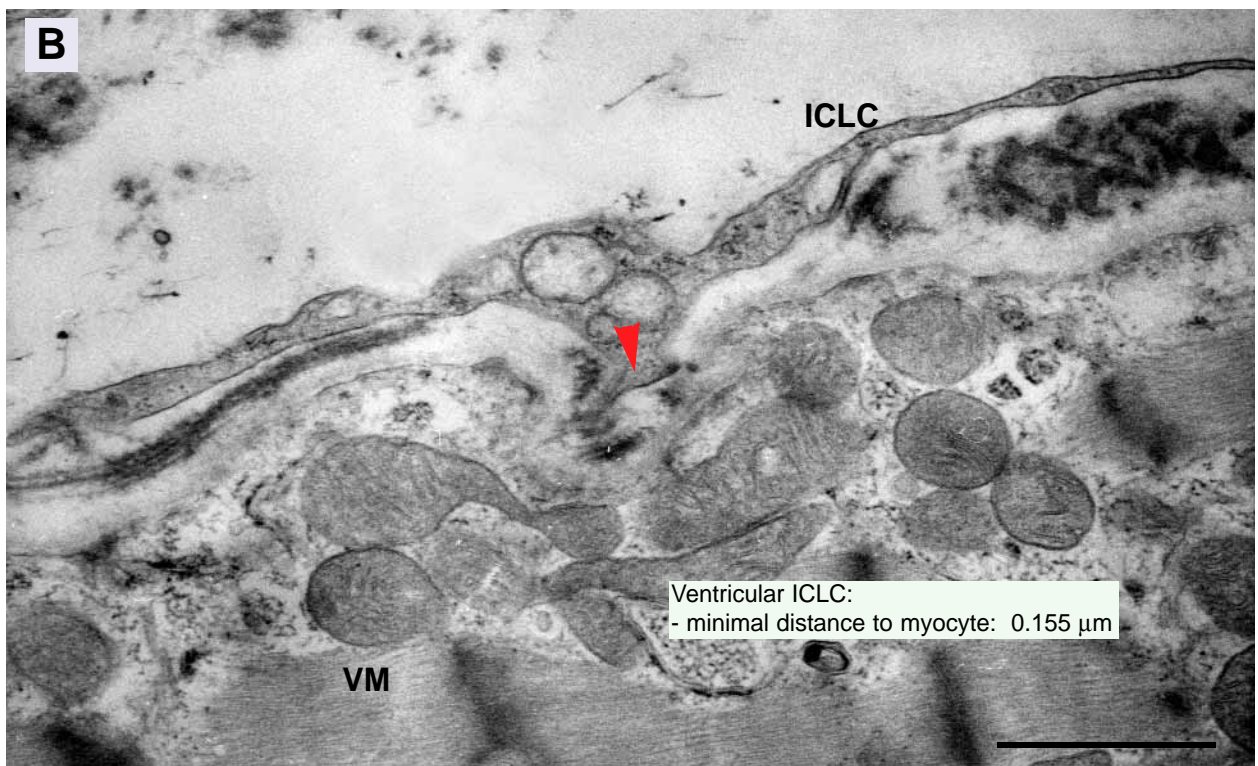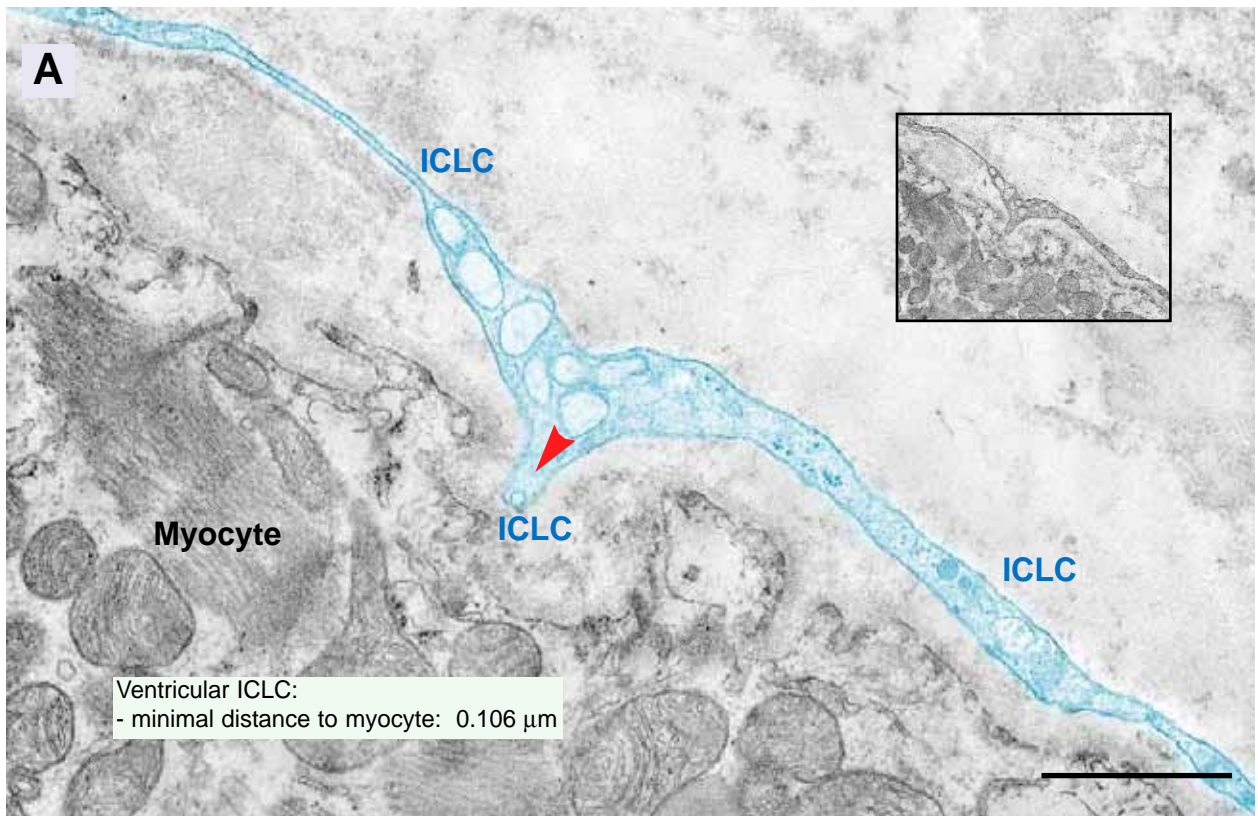
444

Fig. 18 A, B. Two special approach zones between ICLC and ventricular muscle cells. A short ICLC cytoplasmic protrusion, topped by a caveolae (in **A**), is directed to a sarcoplasmalemal depression. Scale bar = 1 μm.
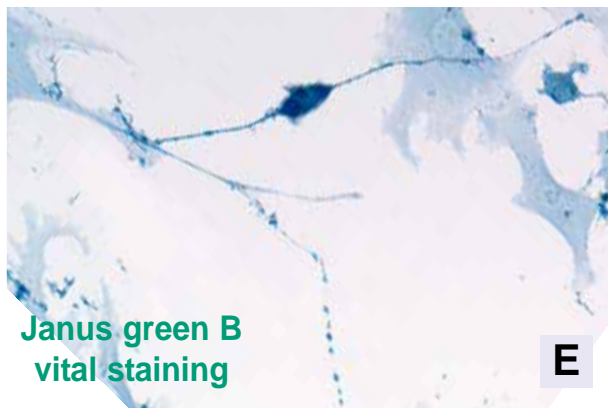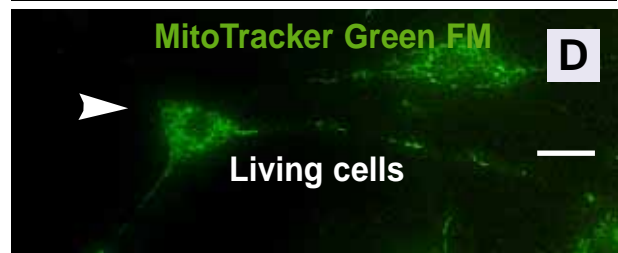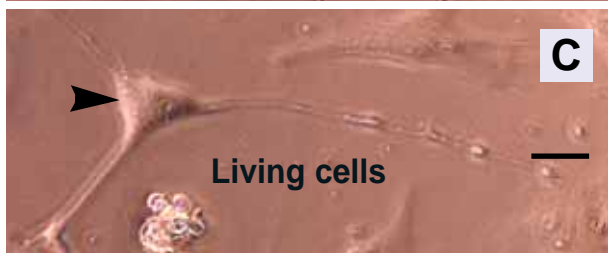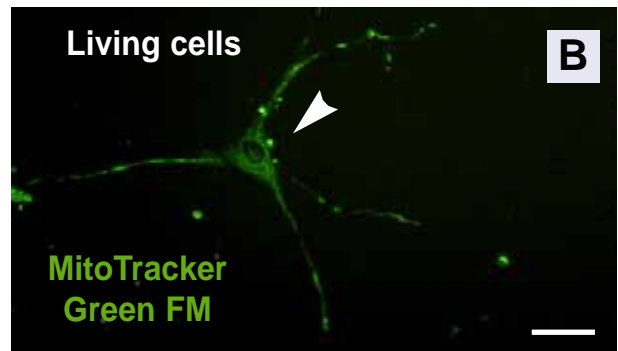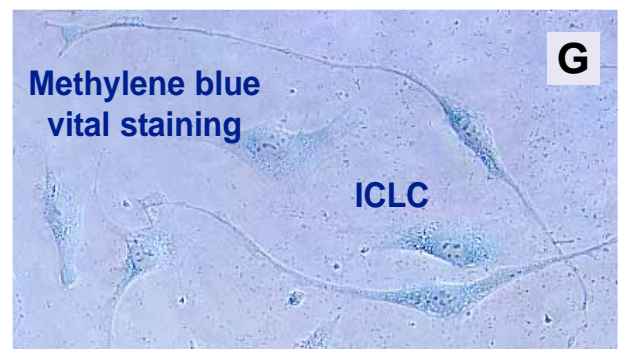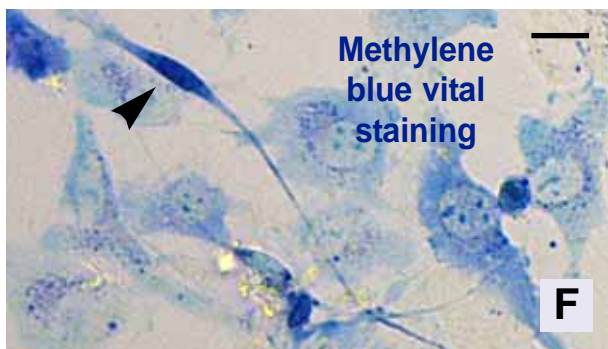
Fig. 19 A–G Rat ventricular myocardium. Interstitial Cajal-like cells (ICLC) isolated in preconfluent primary culture (day 4) as seen in phase contrast microscopy (**A**, **C**) and immunolabelled with a molecular probe for mitochondria (MitoTracker Green FM) displaying a strong staining at prolongation level (**B**, **D**). Janus green B vital staining shows 'beads on a string' appearance of ICLC processes (dilations housing mitochondria) (**E**). Methylene blue vital staining of ICLC (**F, G**). Note the selective darker staining of ICLC with very long, moniliform processes. arrowheads = ICLC. Scale bar = 10 μm.

Results

Identification of ICLC in ventricular myocardial interstitium was based on a set of complementary morphological approaches. Each method was exploited in order to provide data for either the positive or differential diagnosis for ICLC and most of characteristic features were examined comparatively (Fig. 1A, B).

The distribution on cell types of cellular population in ventricular myocardium is presented in Fig. 2 in terms of relative volume.
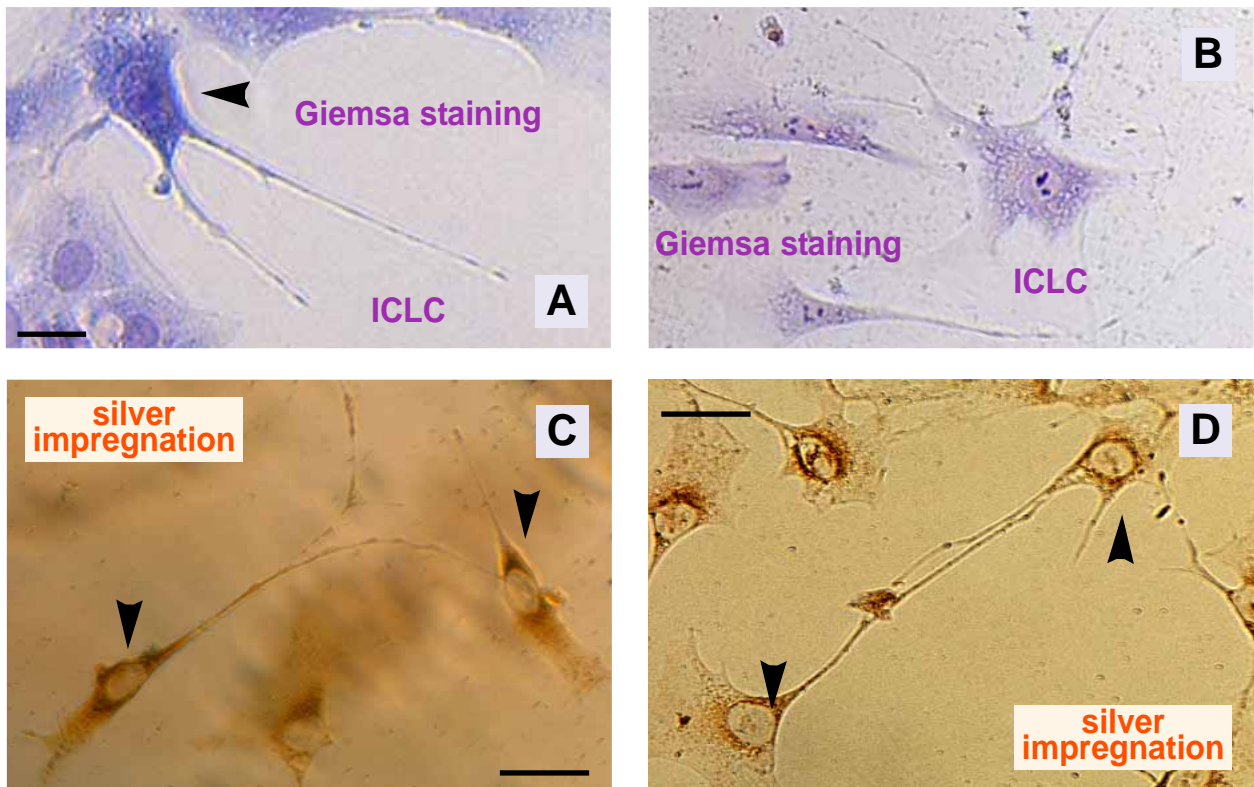
Fig. 20 A–D   Rat ventricular myocardium. Typical interstitial Cajal-like cells (ICLC) isolated in preconfluent primary cultureand stained in magenta with Giemsa method (**A**, **B**). Demonstration of ICLC by silver impregnation (**C**, **D**) Scale bar = 10 µm.
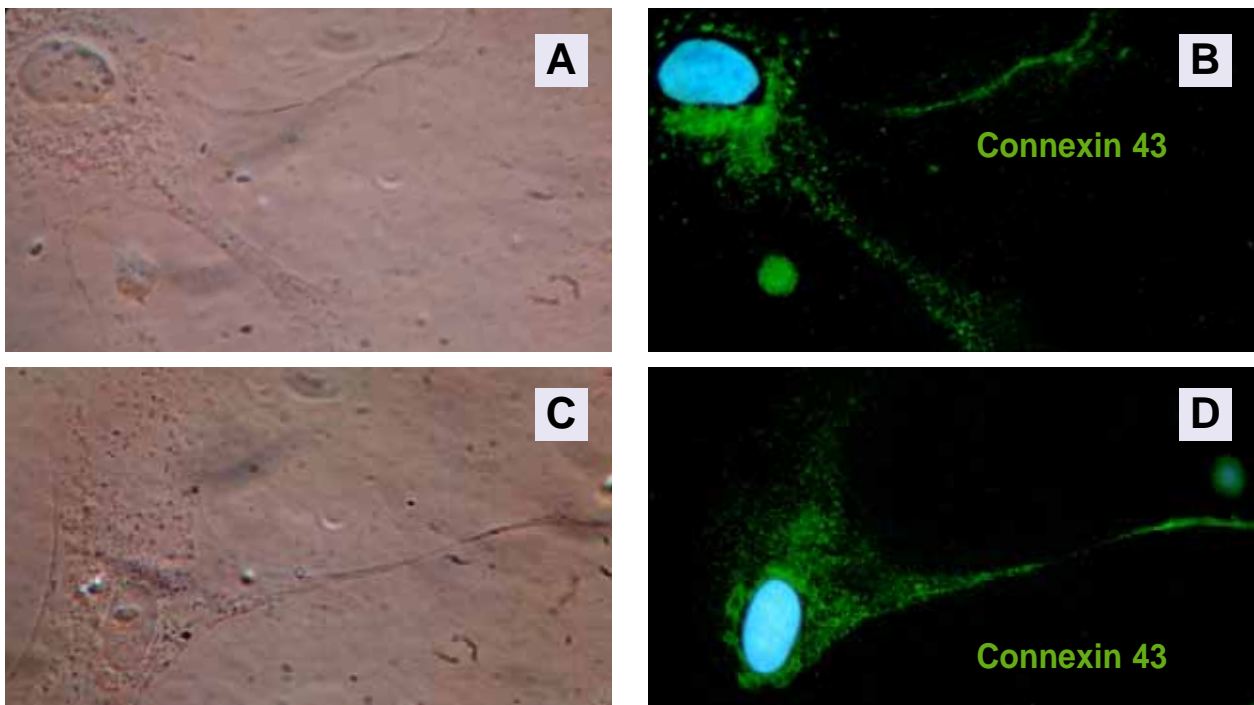

Fig. 21 A–D   Rat ventricular myocardium. Phase contrast microscopy of interstitial Cajal-like cells (ICLC) isolated in preconfluent primary culture (**A**, **C**). Micrographs of same optic fields illustrating immunofluorescence for connexin 43 at ICLC level (cell body and cytoplasmic processes) (**B**, **D**). Scale bar = 10 µm.
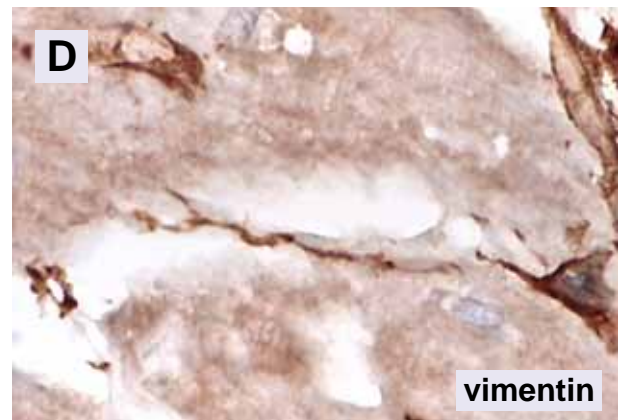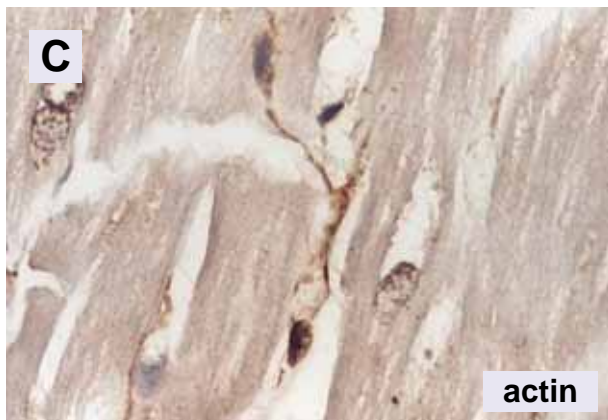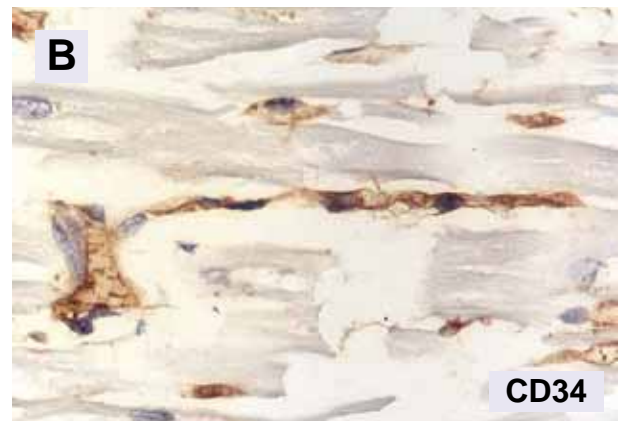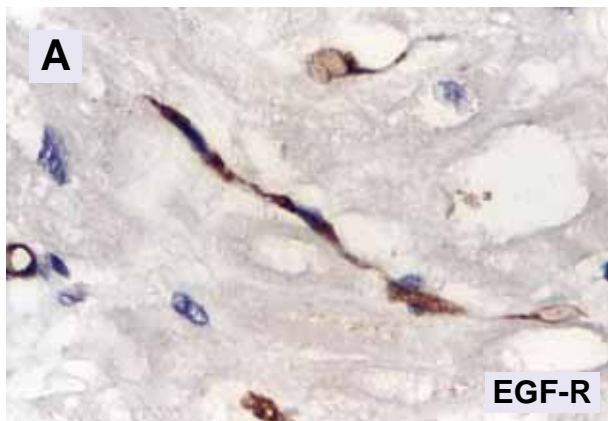
Fig. 22 A–E Human ventricular myocardium. Interstitial Cajal-like cells (ICLC) staining reactivities using different antibodies; avidin-biotin detection (**A–E**).

This chart is based on 20 random photomicrographs on one-micron thick sections stained with toluidine blue and used for quantitative and morphometric analysis of ICLC (*e.g.* total and relative number of cells, number and length of processes etc.) (Fig 3 A-F). This technique revealed the general morphology of ICLC: the cell body and cytoplasmic processes. The close vicinity with capillaries and working myocytes is evident.

Electron microscopy

In order to make ICLC more evident, some TEM images obtained from rat ventricular ultrathin-sections have been digitally colored (Figs. 1A,B; 6A, B; 7, 8A; 12; 13; 14B; 16; 18A). The ultra-

448

Table 1 Comparison of the relative volumes (% of cell volume) occupied by subcellular organelles of ICLC and of fibroblasts in ventricular myocardium.

Subcellular component	Percentage of volume	
	ICLC (n = 9)	Fibroblasts (n = 9)
Nucleus	41.77%	45.36%
Heterochromatin *	29.99%	34.54%
Cytoplasm	58.23%	54.64%
Mitochondria	12.31%	11.48%
Rough endoplasmic reticulum	0.93%	7.89%
Smooth endoplasmic reticulum	1.38%	1.62%
Caveolae	0.93%	0

*   % of nuclear volume

structural criteria for *positive diagnosis*, refined as a 'platinum standard' [17] were examined for each interstitial cell under study. All criteria were fulfilled:

1. *numerous mithochondria* (Figs. 6A, B; 8 A, B; 10 A; 11A,B; 12; 13; 14 A, B; 15; 16);
2. *presence of intermediate filaments* (Fig. 1A);
3. *absence of thick filaments* (Fig. 1; 3-18);
4. *presence of surface caveolae* (Fig. 1A; 5; 6 A, B; 7, 18 A);
5. *variable basal lamina* (Fig. 6A, B);
6. *contacts between ICLC and nerve bundles* (Fig. 9; 12);
7. *presence of smooth and rough endoplasmic reticulum* (Fig. 5);
8. *close apposition with target cells* (Fig. 9; 12; 14B, 17);
9. *specific target(s) in a given organ*, *e.g.* for myocardium: working myocytes (Fig. 4; 8A; 9, 11 A, B; 13; 16), nerve fibres (Fig. 9; 11A; 12; 16, 23 A, B), Schwann cells (14 B; 16); capillaries (Fig. 8B; 9, 13; 14

A-C; 15) or larger arteriolar vessels (Fig. 10 A, B), other connective cells, e.g. fibroblasts (Fig. 11B); Fig. 17 presents a multicontact stromal synapse ('kiss and run') with multiple contact points with a cleft width of ~0.11um, and wider intermembrane distances (0.157-0.239um), as reported previously in atrial myocardium [26].

10. **characteristic cell processes** (Fig. 4; 5; 7A; 8AB; 10 A, B; 11 A,B); the characteristic labyrinthic system of cell prolongation is evident in Fig. 4, 5, 8A, 10A.

The *differential diagnosis* with cardiac working myocytes is easiest, since the histological appearance of the two cell types is very different. The differential diagnosis between ICLC and other interstitial cells may be sometimes be difficult. However, the following criteria allow the distinction: a) *cell shape*: stellate (fig. 5); spindle-shaped (Fig. 7) pyriform (Fig. 8 B), or triangular (Fig. 9, 24 A, B); b) *distinctive ultrastructure of cell processes* (particularly long thin processes, sometimes moniliform, (Fig. 4; 5; 7A; 8AB; 10 A,
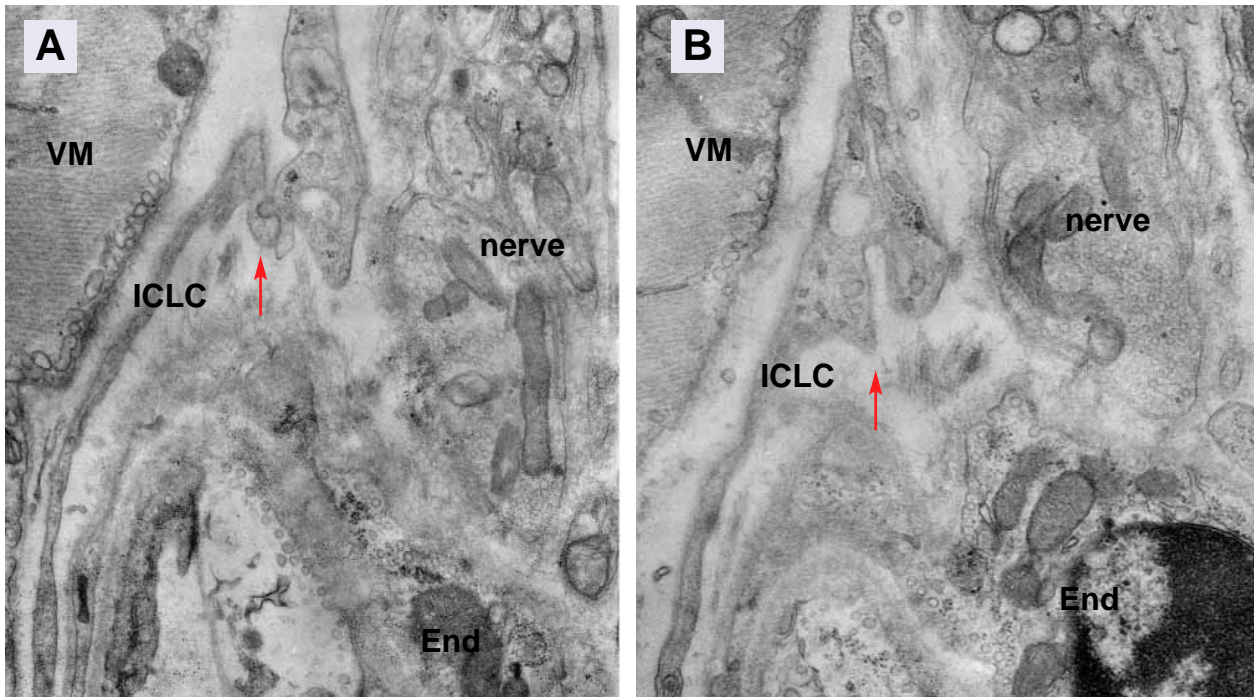
Fig. 23, A and **B** - A little distant two serial sections through a pericapillary space containing an ICLC having close interrelations with nerves. Comparing the two levels of the ICLC profile one can see differences in thickness and foldings, thus helping to get a general idea on the cellular shape.
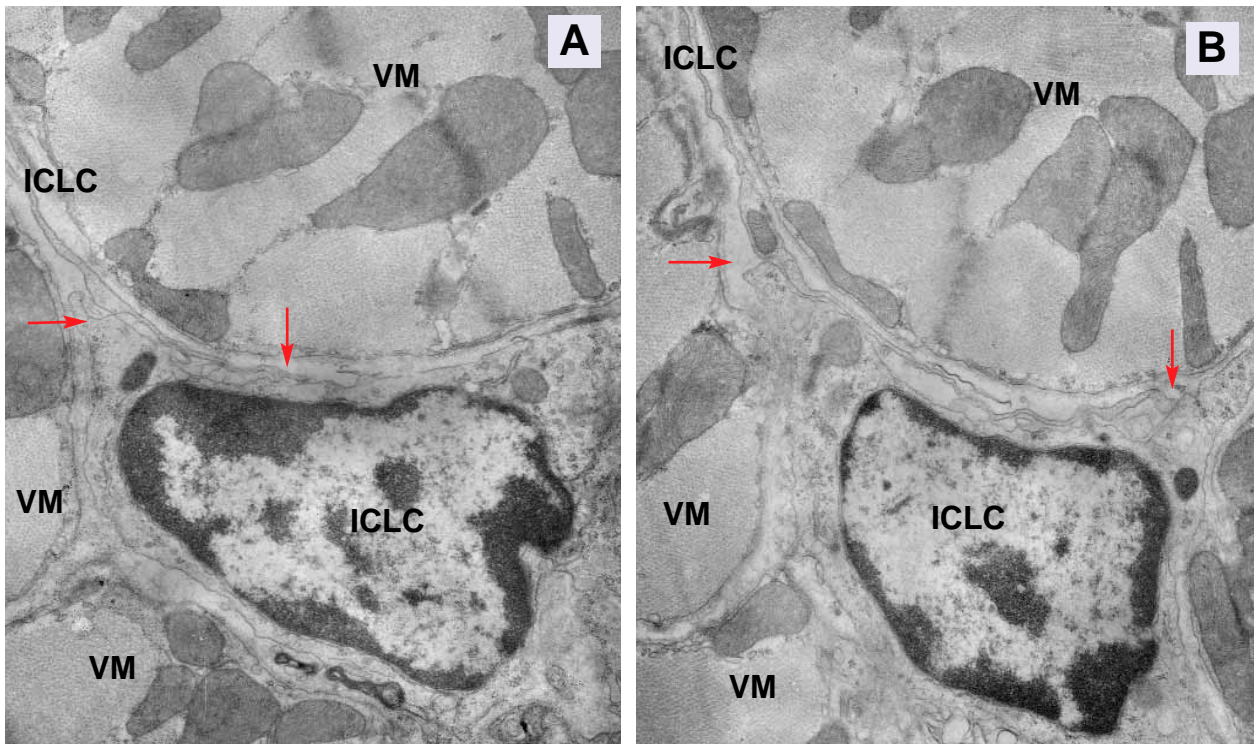
Fig. 24, A and **B** - Two serial, but not consecutive sections showing the close interrelation between an ICLC cytoplasmic veil and another interstitial cell. There are no sites of continuities or junctions between the two cells.

450

B; 11 A,B), c) *positioning in the interstitium* (close vicinity of intrinsic nerve fibers, capillaries, myocytes or other connective cells) (Fig. 4, 8A, B; 9, 10A, B; 11A,B; 12; 13; 14A-C; 15-17.

ICLC *profile* around single or multiple myocardial bundles, nerve fibers or capillaries appears evident in Figs. 6A, B. However, less such enclosing ICLC were observed in ventriculum by comparison with atrial myocardium [25, 26]. Sometimes, a peculiar aspect of cell processes was observed, with a 'wing of a bird' appearance (Fig. 18 A, B). Cardiomyocyte ultrastructure was normal (Fig. 4; 8A; 9, 11 A, B; 13; 16). ICLC show characteristic 1–3 cell processes (Fig. 4; 5; 7A; 8AB; 10 A, B; 11 A,B), with a length of ten of micrometers (Fig. 4, 5, 6A, B), a thickness of ICLC cell processes between ∼ 0.12 μm (Fig. 5, 8A, B, 10 A) and 0.27 μm (Fig. 4). Average *distances from ICLC processes to myocytes* were similar with those observed in atrial myocardium {25, 26]: ∼0.06 μm (Fig. 9), ∼0.11-0.15 μm (Fig. 15, 18 A, B), ∼ 0.20 μm (Fig. 6), ∼0.27-0.29 μm (Fig. 4, 10B), ∼0.34 μm (Fig. 8B), 0.65 μm (Fig. 7) . Measured distances to *endothelial cells* were: ∼ 0.10 μm (Fig. 9, 10A) 1.99 μm (Fig. 8A); 0.34 μm (Fig. 8B); 0.48 μm (Fig. 15). Similarly, distances toward nerve cells were ∼0.10 μm (Fig. 12). Typical labyrinthic systems of long cellular processes are presented in Fig. 4, 5, 8A, 10A. Fig. 9 and 12 illustrate the close relationships of ICLC and nerve fibres in normal ventricular interstitium.

Quantitatively, preliminary estimations revealed that, apparently, there are no significant differences between the left and right ventricle in ICLC distribution. However, ventricular ICLC are clearly less numerous than similar cells in atrial myocardium. Table 1 (p. 449) comparatively presents ultrastructural quantitative details for ICLC and fibroblasts.

Immunohistochemistry

Under our experimental conditions, ICLC were slightly and inconsistently positive for *CD117/c-kit*. However, this should be not taken a a definite truth for *CD117/c-kit*, at this level. Sometimes the

results were in the category which are usually shown in IHC tables as +/- [14,16]. ICLC variously co-expressed *EGF receptor* and *CD34* (Fig. 22A,B), but appeared strongly positive for *vimentin*, along their prolongations (Fig. 22D). Some ICLC seemed positive for *α-smooth muscle actin* (Fig. 22C), or *S-100* (Fig. 22E) but were negative for *nestin*, *desmin*, *CD57*, *tau*, *chymase*, *tryptase* and *CD13*. One may observe that there is a lack of a specific marker for fibroblasts [33] and, on the other hand, most specific immunomarkers for mast cells (chymase or tryptase) for nerve cells (tau, S-100), myofibroblasts, or markers for transdifferentiations (α-smooth muscle actin [34]) were not clearly positive in ICLC. Moreover, it is also noteworthy that IHC alone cannot provide an accurate discrimination among cells in interstitium.
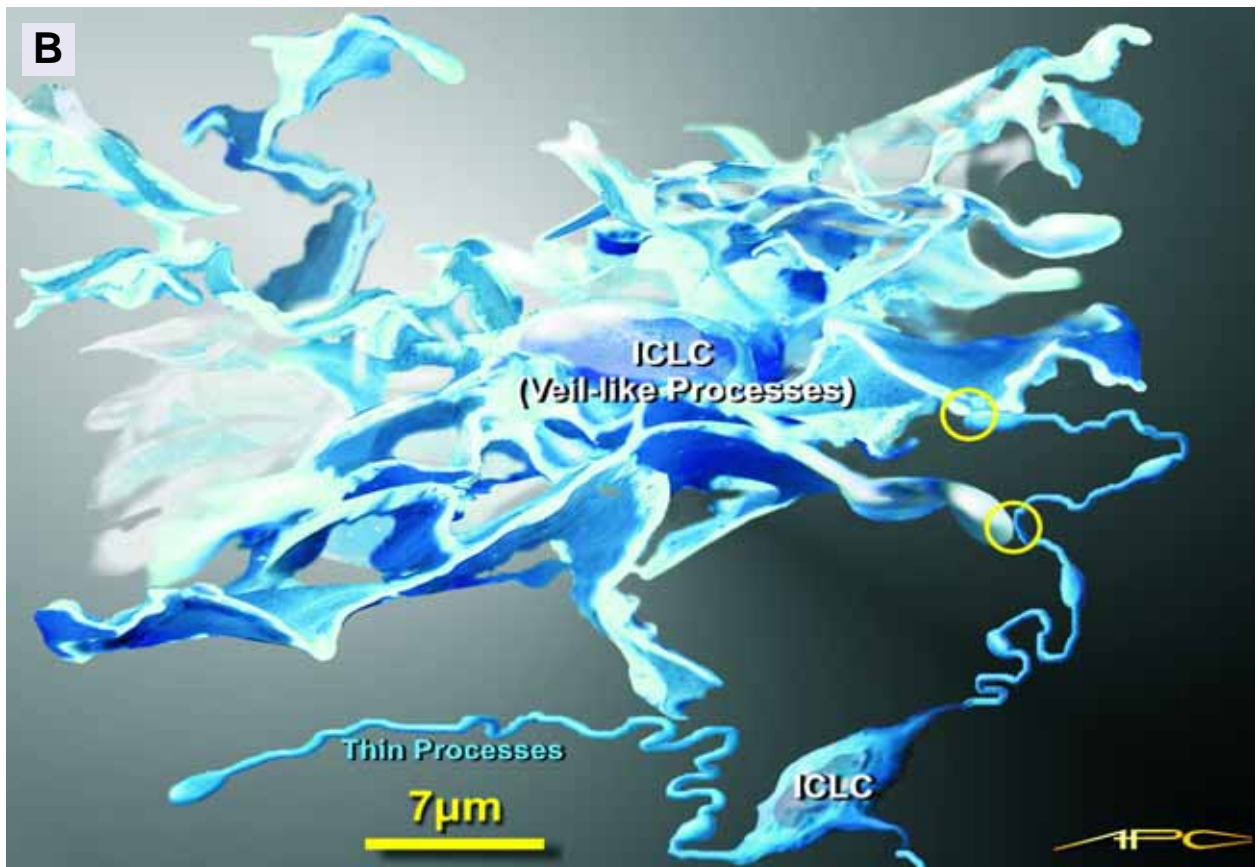
Immunofluorescence

In order to further characterize the long cell prolongations of the interstitial ventricular cells in culture, a molecular probe specific for mitochondria (MitoTracker Green FM) revealed an intense immunopositivity (Fig. 19 B,D). These results correlate well with phase contrast microscopy (Fig. 19 A,C) and TEM data (Fig. 4; 5; 7A; 8AB; 10 A,B; 11 A,B).

We used a two-step procedure whereby unlabeled antibodies against connexin-43 were first bound to their targets, in cultured rat ventricular interstitial cells, and subsequently were detected with fluorochrome-conjugated antibodies (Fig. 21 B,D). By these means the presence of gap junctions demonstrated by TEM was confirmed by an alternative method (connexin-43 presence). It is noteworthy that in our study connexin 43 expression was positive in an ICLC-enriched cell culture, devoid of endothelial cells [35] and in the absence of working myocytes, excluding the gap junctions between working cells [36] or electrocoupling of myocytes and fibroblasts [37].

Stainings in cell cultures

ICLC were successfully maintained in primary culture and can easily be identified before reach-

A

Nerve

Fibroblast

Ventricular Muscle Fiber

Collagen Fibers

Schwann Cell

Axons

Lymphocyte

Capillary

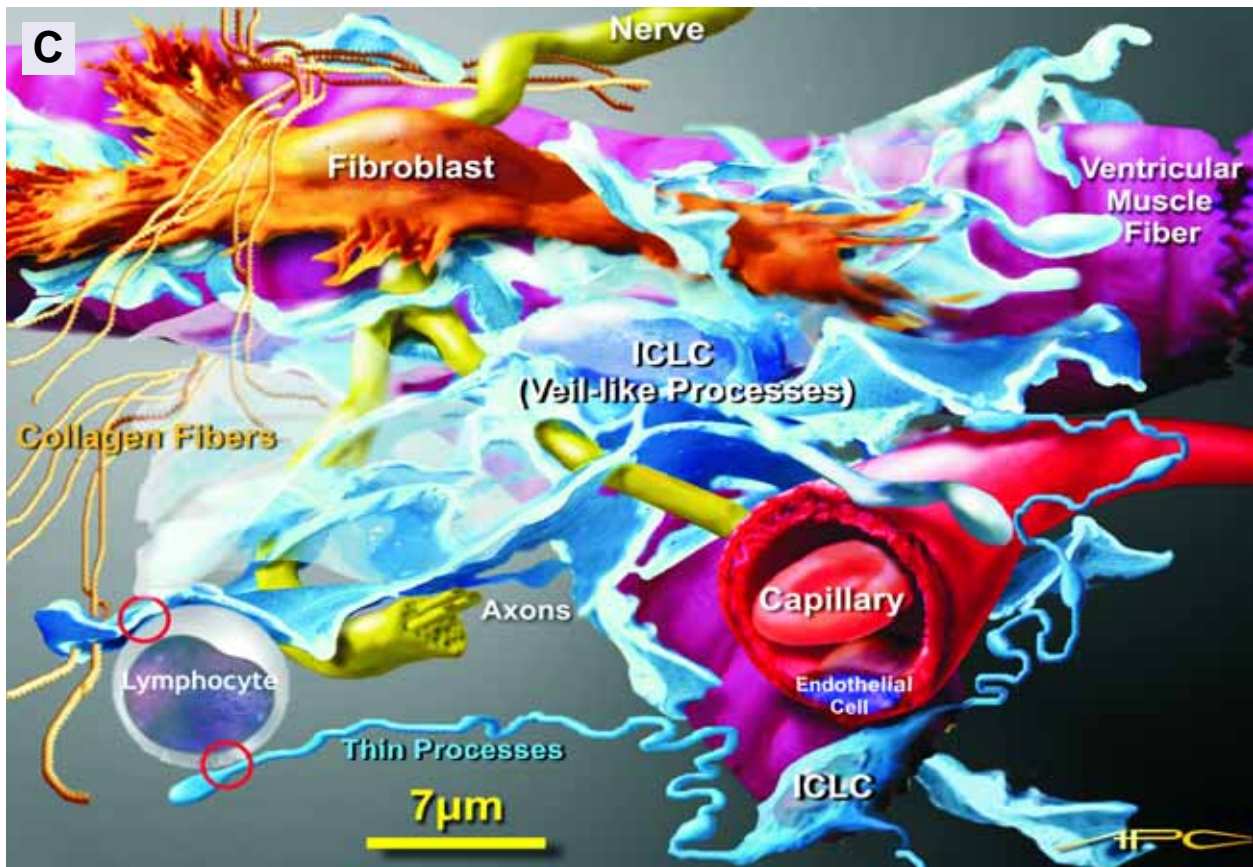Endothelial Cell

7μm

B

ICLC (Veil-like Processes)

Thin Processes

ICLC

7μm
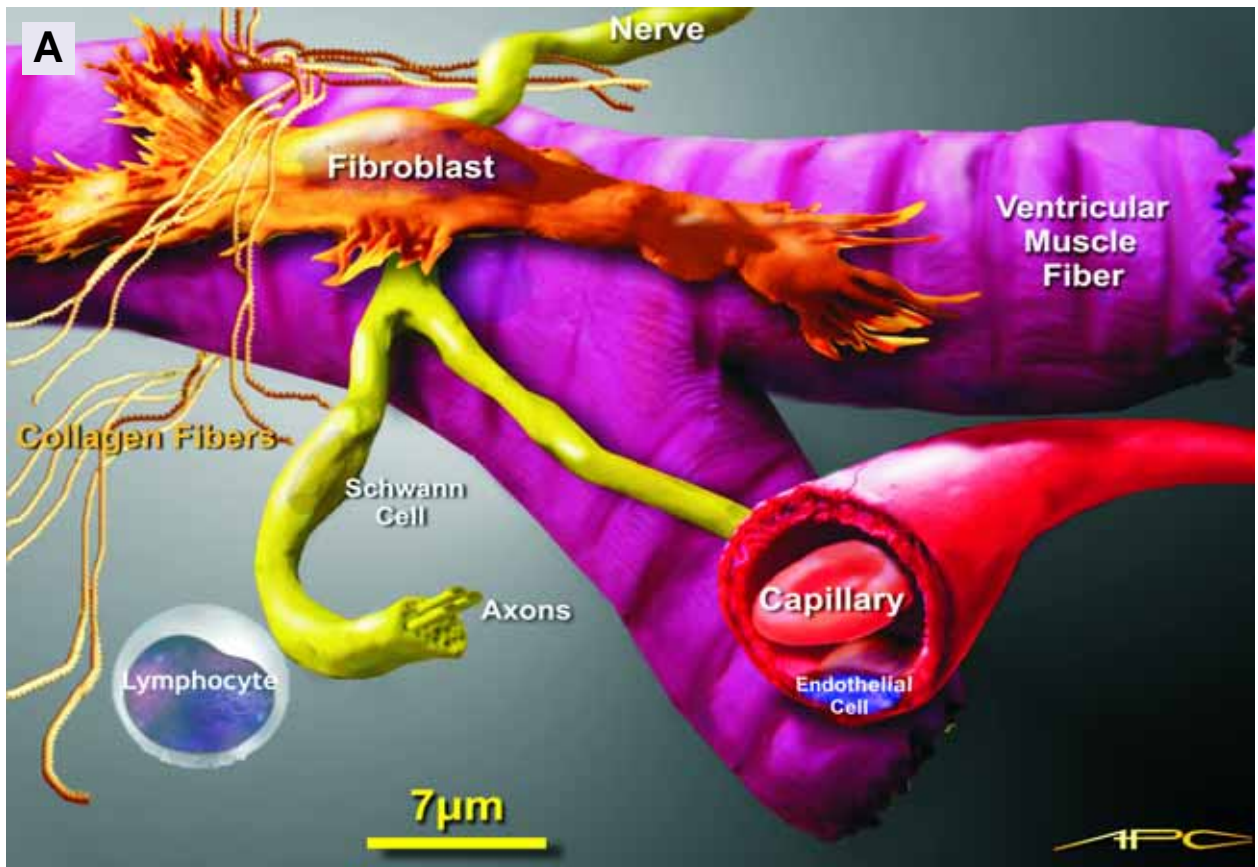
Fig. 25 A. Myocardial background (muscle working cells, capillaries, nerves and fibroblasts). **B. ICLC 'clouds'**, in the interstitial space, floating over the myocardial background. Two possible ways to imagine the ICLC in 3D: '**stratus**'-like thin, broad, perforated veil-like processes and '**cirrus**'-like very long, thin processes. ○ Note the close apposition (gap junctions) between processes of vicinal ICLCs. **C.** Superimposed B over A images: **real landscape (!?)**. Close proximity of ICLC processes and ventricular muscle cell, unmielinated nerves, capillaries, collagen fibers and immunoreactive cells. ○ Stromal synapse. Scale bar - aproximately 7 μm (erytrocyte's diameter).

ing confluence. *Starting with the 3rd day in culture, ICLC appear with long, moniliform processes* (Fig 19). We used **Giemsa stain** to recognize cultured ICLC, since this stain is a mixture containing methylene-blue eosinate and methylene-blue chloride, dissolved in methyl alcohol, with glycerol as a stabiliser (Fig. 20, A, B). We searched for the characteristic moniliform aspect of ICLC processes using *vital stains*: methylene blue (Fig. 19F, G), and Janus green B (Fig. 19E). Vital staining with **methylene blue** revealed that in *living cells*, ICLC processes are very long (several tens of μm), have an uneven caliber, with dilated portions, resembling 'beads on a string'.

TEM studies showed that the dilated portions of the long processes, frequently accomodate mitochondria (Fig. 4; 5; 7A; 8AB; 10 A, B; 11 A,B). **Janus green B** is a well-known *vital stain, with high affinity for mitochondria* [38] and was used to assess viability and localize mitochondria. The initial dark green-blue color, due to mitochondria stained with Janus green B, became a brownish gray one, and finally decolorized (leucocompound) (Fig. 19E) illustrates the staining of ICLC body and dilations of the processes.

Silver impregnation in cell culture evidentiates the thin, long cell prolongations with a beads on a string appearance (Fig. 20 C,D).

Table 2 Examples of ventricular myocardium electron micrographs published during the last 40 years: such images contain cellular 'fragments' or prolongations suggestive for ICLC. The information in this table is based on a routine search of the scientific literature and it should **not** be considered as exhaustive.

Year	Author(s)	Illustration	Positioning	Comment on 'putative' ICLC	Reference
1964	Karnovsky MJ	Fig. 1 (+/-), Fig. 8	Rat ventriculum	No	[39]
1970	Sperelakis N	Fig. 12b	Cat ventriculum	No	[40]
1972	Rumyantsev PP	Fig. 9	Rat ventriculum	No	[41]
1973	Tomanek RJ & Karlsson UL	Fig. 11 (+/-)	Rat ventriculum	No	[42]
1974	Arluk DJ & Rhodin JA	Fig. 4	Calf interventricular septum	Fibroblast	[43]
1975	Maron BJ *et al.*	Fig. 8	Human myocardium from patients with aortic valve disease	No	[44]
1976	Smith HE & E Page	Fig. 5, 6	Rat ventriculum	No	[45]
1977	Jones M & Ferrans VJ	Fig. 9, 10, 13	Crista supraventricularis in patients with tetralogy of Fallot	No	[46]
1977	Schaper W & Schaper J	Fig. 3	Not precised	No	[47]
1979	Spotnitz WD *et al.*	Fig. 6A, B	Immature and adult dog ventriculum	No	[48]
1982	Frank JS *et al.*	Fig. 4	Rabbit interventricular septum	No	[49]
1996	Hayashi T *et al.*	Fig. 4	Human right (ventriculum endomyocardial biopsy)	No	[50
1997	Thornell LE *et al.*	Fig. 4 A,C, 5A, 7B,C, 9A, 10C	Desmin knock-out mouse ventriculum	Interstitial cells	[51]
1998	Schwarz ER *et al.*	Fig. 2A	Human ventriculum (transmural biopsy specimens)	No	[52]
1999	Becker LC *et al.*	Fig. 2A	Dog ventricular myocardium	No	[53]
1999	Hegstad C *et al.*	Fig. 6	Rat ventricular myocardium	No	[54]
2000	Chen C	Fig. 5	Pig ventricular myocardium	No	[55]
2003	Hayashi T *et al.*	Fig. 2B	Diabetic rat ventriculum	No	[56]
2004	Milei J *et al.*	Fig. 2A	Human ventriculum	No	[57]
2006	Wang GY *et al.*	Fig. 2A	Mouse right ventricular trabeculae	No	[58]

Fig. 25 shows an artist's view of the interstitial landscape with and without ICLC in place. Diversity of cell apppearance on TEM micrographs is easier to understand when one looks at the quasi-tridimensional drawing of ICLC alone in Fig. 25B.

Discussion

This study provides extensive morphological proof for the presence of ICLC in human and rat ventricular myocardium. Table 2 presents [based on refs. 39–58] a search of the literature suggesting (but overlooking) the occurence of ICLC or ICLC cell-processes, in ventricular myocardium. According to actual criteria for ultrastructural diagnosis [1, 2, 18], such cells or cell fragments can now be classified as ICLC. Similarly, cells described in this study meet these criteria. As previously discussed for atrial ICLC, perhaps the most controversial area in differential diagnosis of interstitial cells is to make a distinction between ICLC and fibroblasts (or myofibroblasts).

It was documented that 'fibroblasts are principally motile cells and contain actin (mainly α-smooth muscle actin) and myosin' [59]. The absence of thick filaments might signify another piece of evidence supporting the diagnosis of ICLC. *In situ* ICLC have caveolae (while fibroblasts have caveolae only in cell culture), the rough endoplasmic reticulum is much less abundant than in fibroblasts, and additional arguments are the presence of basal lamina, and distinctive cell processes for ICLC. Myofibroblasts are 'not a typical component of normal untraumatised tissues' [60]. However, structural remodeling of the myocardium may be accompanied by the appearance of myofibroblasts [60]. In our opinion, the ultrastructural requisite criteria for myofibroblasts [60–62] are not accomplished in the case of ventricular ICLC: (a) stress fibers; (b) cell-to-stroma attachment sites (fibronexuses); (c) intercellular intermediate (adherens) and gap junctions. However, a gradual increase of fibroblasts/myocyte ratio has been reported in heart disease conditions and myofibroblasts showed abundant expression of α-SMA, vimentin and connexin 43 [63].

The close plasmalemmal appositions that bring ICLC and lymphocyte together in a multicontact type stromal synapse, presented in Fig. 17, provides further support for the 'stromal synapse' concept. We coined and illustrated the term 'stromal synapses' in various organs (between ICLC and immunoreactive cells), supporting the hypothesis that stromal immunoreactive cells are included among the ICLC targets in interstitial intercellular communication [64]. Diagnostic details provided by TEM were, as for atrial ICLC, not available by other approaches. In search for ICLC, IHC anf IF may add value to TEM analysis.

It should be emphasized that the results presented in this article were obtained, in concordance, in three different laboratories, in three different Institutions.

Conclusion

This paper continues a series documenting the occurence of ICLC in human and rat (atrial and ventricular) myocardial interstitium [25, 26].

As concerns possible function, it seems attractive to think that ICLC might participate in the process of cardiac repair/remodeling, arrhythmogenesis and, eventually, sudden death.

Acknowledgments

References

1. **Huizinga JD, Thuneberg L, Vanderwinden JM, Rumessen JJ.** Interstitial cells of Cajal as targets for pharmacological intervention in gastrointestinal motor disorders. *Trends Pharmacol Sci.* 1997; 18: 393-403.

2. **Komuro T, Seki K, Horiguchi K.** Ultrastructural characterization of the interstitial cells of Cajal. *Arch Histol Cytol.* 1999; 62:295-316.

3. **Rumessen JJ, Vanderwinden JM.** Interstitial cells in the musculature of the gastrointestinal tract: Cajal and beyond. *Int Rev Cytol.* 2003; 229:115-208.

4. **Faussone-Pellegrini MS.** Interstitial cells of Cajal: once negligible players, now blazing protagonists. *Ital J Anat Embryol.* 2005; 110:11-31.

5. **Faussone-Pellegrini MS.** Relationships between neurokinin receptor-expressing interstitial cells of Cajal and tachykininergic nerves in the gut. *J Cell Mol Med.* 2006; 10:20-32.

6. **Cho WJ, Daniel EE.** Colocalization between caveolin isoforms in the intestinal smooth muscle and interstitial cells of Cajal of the Cav1(+/+) and Cav1 (-/-) mouse. *Histochem Cell Biol.* 2006; 126:9-16.

7. **Hirst GD, Ward SM.** Interstitial cells: involvement in rhythmicity and neural control of gut smooth muscle. *J Physiol.* 2003; 550: 337-46.

8. **Sanders KM, Koh SD, Ward SM.** Interstitial cells of cajal as pacemakers in the gastrointestinal tract. *Annu Rev Physiol.* 2006; 68: 307-43.

9. **Huizinga JD, Faussone-Pellegrini MS**. About the presence of interstitial cells of Cajal outside the musculature of the gastrointestinal tract, *J Cell Mol Med.* 2005; 9: 468-73

10. **Popescu LM, Hinescu ME, Ionescu N, Ciontea MS, Cretoiu D, Ardeleanu C.** Interstitial cells of Cajal in pancreas. *J Cell Mol Med.* 2005; 9: 169-90.

11. **Harhun MI, Pucovsky V, Povstyan OV, Gordienko DV, Bolton TB**. Interstitial cells in the vasculature. *J Cell Mol Med.* 2005; 9: 232-43.

12. **Bobryshev YV.** Subset of cells immunopositive for neurokinin-1 receptor identified as arterial interstitial cells of Cajal in human large arteries. *Cell Tissue Res.* 2005; 321: 45-55.

13. **Hashitani H, Suzuki H.** Identification of interstitial cells of Cajal in corporal tissues of the guinea-pig penis. *Br J Pharmacol.* 2004; 141: 199-204.

14. **Ciontea MS, Radu E, Regalia T, Ceafalan L, Cretoiu D, Gherghiceanu M, Braga RI, Malincenco M, Zagrean L, Hinescu ME, Popescu LM.** C-kit immunopositive interstitial cells (Cajal-type) in human myometrium. *J Cell Mol Med.* 2005; 9: 407-20.

15. **Popescu LM, Vidulescu C, Curici A, Caravia L, Simionescu AA, Ciontea SM, Simion S.** Imatinib

16. **Duquette RA, Shmygol A, Vaillant C, Mobasheri A, Pope M, Burdyga T, Wray S.** Vimentin-positive, c-kit-negative interstitial cells in human and rat uterus: a role in pacemaking? *Biol Reprod.* 2005; 72:276-83

17. **Popescu LM, Ciontea SM, Cretoiu D, Hinescu ME, Radu E, Ionescu N, Ceausu M, Gherghiceanu M, Braga RI, Vasilescu F, Zagrean L, Ardeleanu C,** Novel type of interstitial cell (Cajal-like) in human fallopian tube. *J Cell Mol Med.* 2005; 9:479-523

18. **Van der Aa F, Roskams T, Blyweert W, De Ridder D.** Interstitial cells in the human prostate: a new therapeutic target? *Prostate.* 2003; 56: 250-5

19. **Davidson RA, McCloskey KD.** Morphology and localization of interstitial cells in the guinea pig bladder: structural relationships with smooth muscle and neurons. *J Urol.* 2005; 173:1385-90

20. **Brading AF.** Spontaneous activity of lower urinary tract smooth muscles: correlation between ion channels and tissue function. *J Physiol.* 2006; 570:13-22

21. **Gherghiceanu M, Popescu LM.** Interstitial Cajal-like cells (ICLC) in human resting mammary gland stroma. Transmission electron microscopy identification. *J Cell Mol Med.* 2005; 9: 893-910

22. **Lang RJ, Klemm MF.** Interstitial cells of Cajal-like cells in the upper urinary tract, *J Cell Mol Med.* 2005; 9: 543-556

23. **Sergeant GP, Thornbury KD, McHale NG, Hollywood MA.** Interstitial cells of Cajal in the urethra, *J Cell Mol Med.* 2006; 10: 280-291

24. **Adler CP, Friedburg H, GW Herget, Neuburger M Schwalb H**, Variability of cardiomyocyte DNA content, ploidy level and nuclear number in mammalian hearts, *Virchows Arch* 1996; 429: 159-64

25. **Hinescu ME, Popescu LM,** Interstitial Cajal-like cells (ICLC) human atrial myocardium, *J Cell Mol Med* 2005; 9: 972-5

26. **Hinescu ME, Gherghiceanu M, Mandache E, Ciontea SM, Popescu LM.** Interstitial Cajal-like cells (ICLC) in atrial myocardium: ultrastructural and immunohistochemical characterization, *J Cell Mol Med* 2006; 10: 243-257

27. **Weibel E.R.,** Practical methods for biological morphometry. Stereological methods, London, Academic Press, 1979

28. **Hsu SM, Raine L, Fanger H.** Use of avidin-biotin-peroxidase complex (ABC) in immunoperoxidase techniques: a comparison between ABC and unlabeled antibody (PAP) procedures. *J Histochem Cytochem.* 1981; 29: 577-80

29. **Bussolati G, Gugliotta P.** Nonspecific staining of mast cells by avidin-biotin-peroxidase complexes (ABC). *J Histochem Cytochem.* 1983; 31: 1419-21

inhibits spontaneous rhythmic contractions of human uterus and intestine. *Eur J Pharmacol.* 2006; doi:10.1016/j.ejphar.2006.06.068.

30. **Mora R, Bonilha VL, Marmorstein A, Scherer PE, Brown D, Lisanti MP, Rodriguez-Boulan E.** Caveolin-2 localizes to the golgi complex but redistributes to plasma membrane, caveolae, and rafts when co-expressed with caveolin-1. *J Biol Chem.* 1999; 274: 25708-17

31. **Keij JF, Bell-Prince C, Steinkamp JA.** Staining of mitochondrial membranes with 10-nonyl acridine orange, MitoFluor Green, and MitoTracker Green is affected by mitochondrial membrane potential altering drugs. *Cytometry.* 2000; 39: 203-10

32. **Vanden Berghe P, Hennig GW, Smith TK.** Characteristics of intermittent mitochondrial transport in guinea pig enteric nerve fibers. *Am J Physiol Gastrointest Liver Physiol.* 2004; 286: G671-82

33. **Goldsmith EC, Hoffman A, Morales MO, Potts JD, Price RL, McFadden A, Rice M, Borg TK.** Organization of fibroblasts in the heart. Dev Dyn. 2004; 230: 787-94

34. **Paranya G, Vineberg S, Dvorin E, Kaushal S, Roth SJ, Rabkin E, Schoen FJ, Bischoff J.** Aortic valve endothelial cells undergo transforming growth factor-beta-mediated and non-transforming growth factor-beta-mediated transdifferentiation *in vitro. Am J Pathol.* 2001; 159: 1335-43

35. **Narmoneva DA, Vukmirovic R, Davis ME, Kamm RD, Lee RT.** Endothelial cells promote cardiac myocyte survival and spatial reorganization: implications for cardiac regeneration. *Circulation.* 2004; 110: 962-8

36. **Tribulova N, Dupont E, Soukup T, Okruhlicova L, Severs NJ.** Sex differences in connexin-43 expression in left ventricles of aging rats. *Physiol Res.* 2005; 54:705-8

37. **Kohl P, Camelliti P, Burton FL, Smith GL.** Electrical coupling of fibroblasts and myocytes: relevance for cardiac propagation. *J Electrocardiol.* 2005; 38: 45-50

38. **Lazarow A, Cooperstein SJ.** Studies on the enzymatic basis for the Janus green B staining reaction. *J Histochem Cytochem.* 1953; 1: 234-41.

39. **Karnovsky MJ**, The localization of cholinesterase activity in rat cardiac muscle by electron microscopy, 1964 *J Cell Biol* 23:217-32

40. **Sperelakis N, Rubio R, Redick J.** Sharp discontinuity in sarcomere lengths across intercalated disks of fibrillating cat hearts. *J Ultrastruct Res.* 1970;30:503-32 (de verificat referinta)

41. **Rumyantsev PP,** Electron microscope study of the myofibril partial disintegration and recovery in the mitotically dividing cardiac muscle cells. 1972; *Z Zellforsch* 129:471-99

42. **Tomanek RJ, Karlsson UL,** Myocardial ultrastructure of young and senescent rats. *J Ultrastruct Res.* 1973;42:201-20

43. **Arluk DJ, Rhodin JA.** The ultrastructure of calf heart conducting fibers with special reference to nexuses and their distribution. *J Ultrastruct Res.* 1974; 49:11-23

44. **Maron BJ, Ferrans VJ, Roberts WC**, Myocardial ultrastructure in patients with chronic aortic valve disease. *Am J Cardiol.* 1975;35:725-39

45. **Smith HE, Page E**, Morphometry of rat heart mitochondrial subcompartments and mebranes: application to myocardial cell atrophy after hypophysectomy, 1976; *J Ultrastruct Res* 55:31-41

46. **Jones M, Ferrans VJ.** Myocardial degeneration in congenital heart disease. Comparison of morphologic findings in young and old patients with congenital heart disease associated with muscular obstruction to right ventricular outflow. *Am J Cardiol* 1977;39:1051-63

47. **Schaper W, Schaper J**. The coronary microcirculation. Am J Cardiol. 1977;40:1008-12

48. **Spotnitz WD, Spotnitz HM, Truccone NJ, Cotrell TS, Gersony W, Malm JR, Sonnenblick EH**, Relation of ultrastructure and function, 1979; *Circ Res* 44:679-91

49. **Frank JS, Rich TL, Beydler S, Kreman M**, Calcium depletion in rabbit myocardium. Ultrastructure of the sarcolemma and correlation with the calcium paradox. *Circ Res* 1982;51:117-30

50. **Hayashi T, Okamoto F, Terasaki F, Deguchi H, Hirota Y, Kitaura Y, Spry CJF, Kawamura K,** Ultrastructural and immunohistochemical studies on myocardial biopsies from a patient with eosinophilic endomyocarditis *Cardiovasc Pathol* 1996 ;5:105-112

51. **Thornell L, Carlsson L, Li Z, Mericskay M, Paulin D**, Null mutation in the desmin gene gives rise to a cardiomyopathy, *J Mol Cell Cardiol* 1997; 29:2107-24

52. **Schwarz ER, Schoendube FA, Kostin S, Schmiedtke N, Schulz G, Buell U, Messmer BJ, Morrison J, Hanrath P, vom Dahl J.** Prolonged myocardial hibernation exacerbates cardiomyocyte degeneration and impairs recovery of function after revascularization. *J Am Coll Cardiol.* 1998;31:1018-26

53. **Becker LC, Jeremy RW, Schaper J, Schaper W.** Ultrastructural assessment of myocardial necrosis occurring during ischemia and 3-h reperfusion in the dog. *Am J Physiol.* 1999;277:H243-52

54. **Hegstad AC, Ytrehus K, Lindal S, Jorgensen L.** Ultrastructural alterations during the critical phase of reperfusion: a stereological study in buffer-perfused isolated rat hearts. *Cardiovasc Pathol.* 1999; 8:279-89.

55. **Chen C, Liu J, Hua D, Ma L, Lai T, Fallon JT, Knibbs D, Gillam L, Mangion J, Knight DR, Waters D**. Impact of delayed reperfusion of myocardial hibernation on myocardial ultrastructure and function and their recoveries after reperfusion in a pig model of myocardial hibernation. *Cardiovasc Pathol* 2000;9:67-84

56. **Hayashi T, Sohmiya K, Ukimura A, Endoh S, Mori T, Shimomura H, Okabe M, Terasaki F, Kitaura Y** Angiotensin II receptor blockade prevents microangiopathy and preserves diastolic function in the diabetic rat heart. *Heart* 2003 ;89:1236-42

57. **Milei J, Fraga CG, Grana DR, Ferreira R, Ambrosio G.** Ultrastructural evidence of increased tolerance of hibernating myocardium to cardioplegic ischemia-reperfusion injury. *J Am Coll Cardiol* 2004; 43:2329-36

58. **Wang GY, Bergman MR, Nguyen AP, Turcato S, Swigart PM, Rodrigo MC, Simpson PC, Karliner JS, Lovett DH, Baker AJ,** Cardiac transgenic matrix metalloproteinase-2 expression directly induces impaired contractility. *Cardiovasc Res.* 2006, 15;69:688-96

59. **Camelliti P, Borg TK, Kohl P.** Structural and functional characterisation of cardiac fibroblasts. *Cardiovasc Res.*2005; 65:40-51

60. **Eyden B.** The myofibroblast: a study of normal, reactive and neoplastic tissues, with an emphasis on ultrastructure. Part 1—normal and reactive cells. *J Submicrosc Cytol Pathol.* 2005, 37: 109-204

61. **Eyden B.** The myofibroblast: an assessment of controversial issues and a definition useful in diagnosis and research. *Ultrastruct Pathol.* 2001; 25: 39-50

62. **Rabkin E, Aikawa M, Stone JR, Fukumoto Y, Libby P, Schoen FJ.** Activated interstitial myofibroblasts express catabolic enzymes and mediate matrix remodeling in myxomatous heart valves. *Circulation.* 2001;104: 2525-32

63. **Miragoli M, Gaudesius G, Rohr S.** Electrotonic modulation of cardiac impulse conduction by myofibroblasts. *Circ Res.* 2006; 98: 801-10

64. **Popescu LM, Gherghiceanu M, Cretoiu D, Radu E.** The connective connection: interstitial cells of Cajal (ICC) and ICC-like cells establish synapses with immunoreactive cells. Electron microscope study *in situ*. *J Cell Mol Med.* 2005; 9: 714-30